Utrecht University

Department of Mathematics

Bachelor Thesis

Codim 2 bifurcations of planar heteroclinic contours

Joost Hooyman

supervised by
Prof. dr. Yuri A. Kuznetsov

June 11, 2020

Abstract

Smooth planar vector fields containing two hyperbolic saddles may contain contours formed by heteroclinic connections between these saddles. This thesis presents an overview of the bifurcations of these contours based on publications by J.W. Reyn [11] and A. Dukov [7]. Using truncated correspondence maps, all relevant bifurcations diagrams are rederived. Additionally, two new explicit polynomial systems containing such contours are derived which are studied using the bifurcation software Matcont [5, 6, 3].

Contents

Part I
Introduction

1 Overview

Consider a vector field in the plane containing two saddles and suppose an orbit leaving one saddle connects to the other saddle and vice versa. This configuration of saddles and orbits is called a heteroclinic contour. This thesis investigates bifurcations occurring in two-parameter families of vector fields containing such contours.

Heteroclinic contours can be subdivided into two categories, namely monodromic and non-monodromic. For both cases there already exist separate theoretical studies. Results on the monodromic case have been published in 1980 by J.W. Reyn [11] and are quite well known. For example, they are included in the review [2] and reproduced in the encyclopedic work [1]. A much more recent 2018 publication by A. Dukov [7] treats the non-monodromic case.

In both cases, depending on the eigenvalues of the saddles, either one limit cycle or two limit cycles of opposite stability are generated as the result of homoclinic bifurcations. When two limit cycles exist these may collide to form a semi-stable limit cycle at a fold (or saddle-node) of cycles bifurcation.

The non-monodromic case exhibits the additional phenomenon of flashing heteroclinic connections, which may be described as an infinite series of connections from one saddle to the other making arbitrarily many windings around one of the saddles. This phenomenon was already discovered in 1981 by I.P. Malta and J. Palis [10] but in a less general (one-parameter) context. Consequently, the non-monodromic case provides an example of a situation which is only two-dimensional but nevertheless possesses a bifurcation diagram of considerable complexity.

The first aim of this thesis is to collect the results of both papers and present them in a unified way. In this manner, we hope to obtain a polished treatment of the bifurcations of planar heteroclinic contours in both the monodromic as well as the non-monodromic case.

The second aim of this thesis is to derive two polynomial systems which contain heteroclinic connections of the monodromic and non-monodromic kind respectively. These systems may be

perturbed to bifurcate as predicted in the theoretical part.

The method to obtain the monodromic example system is adapted from a method to derive a polynomial system containing a homoclinic connection published in a 1997 paper by B. Sandstede [12]. The non-monodromic example system is derived by modifying a reversible system containing a homoclinic connection.

After these explicit polynomial systems are obtained we use the standard numerical software package MatCont [5, 6, 3] to continue relevant phase objects in two parameters, thus numerically producing bifurcation diagrams of these systems.

1.1 Structure of this thesis

The core of this thesis consists of three parts. Below we will explain the contents of these parts and describe the main techniques used in each part.

In the preparatory first part, *Planar vector fields and bifurcations*, we collect notions necessary to define systems containing heteroclinic contours. Then, the phenomenon of bifurcation is discussed and some relevant bifurcations are introduced, together with the necessary tools to study and describe them.

In the second part, *Bifurcations of heteroclinic contours*, we define the different types of heteroclinic contours (monodromic and non-monodromic) and distinguish two relevant cases to be considered. From here we treat the monodromic and non-monodromic cases separately and discuss the generation homoclinic connections, heteroclinic connections and limit cycles. In both cases this discussion results in producing generic bifurcation diagrams under certain non-degeneracy conditions.

Throughout this part, our main tools will be several model maps, which are truncated maps describing the behaviour of solutions both locally (near the saddles) and globally (along the heteroclinic connections). Composition of these maps yields a model Poincaré map which describes the behaviour of solutions as they move around the heteroclinic contour. Using this map, we will be able to prove all results needed to produce the theoretical bifurcation diagram.

In the third part, *Two polynomial examples*, we derive two polynomial examples. The method to derive a monodromic example is as follows. First, we look for an algebraic set which has a similar shape to a monodromic heteroclinic contour. We choose the union of a horizontal line with a parabola. Then, we look for vector fields

which are tangent to this variety. We try two general second order polynomials as the components of the vector field. This results in a system of three polynomial equations. This system is solved by computing the Gröbner basis of this system, selecting the least complicated basis polynomial and solving in terms of the coefficients to obtain a function, which is identically zero on the union of the line and the parabola. From the resulting conditions on the parameters we obtain a vector field containing a nondegenerate monodromic heteroclinic contour.

To this vector field we add two perturbing terms which respectively leave the horizontal line and the parabola unaffected. Using MatCont we numerically obtain the numerical bifurcation diagram of this system and we supply numerically generated representative phase portraits for all non-critical values of the parameters.

The non-monodromic example system is derived by modifying a reversible system containing a homoclinic connection. To this system we add a two-parameter perturbation. For this example we again use MatCont to obtain several essential curves in the bifurcation diagram. In this case, we supply phase portraits for critical values of the parameters which show homoclinic connections and two of the flashing heteroclinic connections.

1.2 Contributions

We claim that this thesis makes the following contributions to the study of bifurcations of vector fields. Firstly, we revisit and unify two existing theoretical studies [11] and [7]. Secondly, we derive and study two explicit polynomial families of vector fields exhibiting three of the four relevant subcases of bifurcations of planar heteroclinic contours. At present, other publications presenting such explicit examples are not known to us.

1.3 Acknowledgments

First and foremost, I would like to thank my supervisor Prof. dr. Yuri A. Kuznetsov for his guidance, enthousiasm and countless contributions to this thesis. Furthermore, we would like to thank A. Dukov for providing an English translation of his paper [7].

Part II
Planar vector fields and bifurcations

The purpose of this part of the thesis is to supply all necessary definitions and results needed to study bifurcations of heteroclinic contours. The more knowledgeable reader may skip this part or refer only to it when necessary.

We begin by defining the types of systems under consideration and recall how from these systems we arrive at the orbits of these systems which we can draw in the phase-portrait. Next, we discuss the relevant types of orbits which appear in systems containing heteroclinic contours. After the relevant objects appearing in the phase portrait are discussed we discuss the concept of bifurcation and how the bifurcational behaviour of a system may be depicted in a bifurcation diagram. Lastly, we use the defined concepts to discuss all bifurcations which we will encounter in systems containing heteroclinic contours, along with methods to study them.

Much of the treatment in this section is not rigorous. A complete treatment of most topics can be found in [9].

2 Planar vector fields

2.1 Basic definitions

Let $x = (x_1, x_2)$ represent a point in the plane $\mathbb{R}^2$ and consider a system

$$\begin{cases} \dot{x}_1 = P(x_1, x_2), \\ \dot{x}_2 = Q(x_1, x_2), \end{cases} \tag{2.1}$$

where the functions P and Q are smooth functions from $\mathbb{R}^2$ to $\mathbb{R}$. The map $(x_1, x_2) \mapsto (P(x_1, x_2), Q(x_1, x_2))$ is called a ***smooth vector field***. We recall that such a vector field defines, for small values of $t \in \mathbb{R}$ a ***local flow*** $\varphi : \mathbb{R}^2 \times \mathbb{R} \to \mathbb{R}^2$ which can be understood as moving the point $x_0 \in \mathbb{R}^2$ along the vector field for t units of time.

If we denote by $I(x_0) \subseteq \mathbb{R}$ the values of t for which the flow is defined we define the ***orbit*** containing x_0 as

$$\{\varphi(x_0, t) \mid t \in I(x_0)\} \subset \mathbb{R}^2.$$

If we draw a collection of orbits in the plane along with the direction of the vector field we obtain what is called a ***phase portrait***, which at a glance gives an impression of the behaviour of the system.

If we wish to describe the flow starting in a certain point without explicitly mentioning this point we can more generally define a ***solution curve*** as

$$\gamma(t) = \varphi(x_0, t)$$

for some $x_0 \in \mathbb{R}^2$.

2.2 Equilibria and their types

Given the system (2.1), a point $x^0 = (x_1^0, x_2^0)$ satisfying

$$P(x_1^0, x_2^0) = Q(x_1^0, x_2^0) = 0$$

is called an ***equilibrium***. At such a point, the vector field has no direction and it is readily seen that the orbit containing an equilibrium must consist of this equilibrium alone.

Recall that for linear vector fields, seen as linear maps from $\mathbb{R}^2$ to $\mathbb{R}^2$, we can calculate its eigenvalues at any point. At equilibria, these eigenvalues allow us to classify them. We call an equilibrium ***hyperbolic*** if none of its eigenvalues are purely imaginary. Among hyperbolic equilibria we distinguish ***foci*** (both eigenvalues complex), ***nodes*** (both eigenvalues real and with the same sign) and ***saddles*** (both eigenvalues real and of opposing sign).

For general vector fields we may calculate its Jacobian matrix at any point. This matrix defines a linear map which is the best linear approximation of the vector field at this point. The following theorem shows that locally, we may treat the equilibrium as linear.

Theorem 2.1 (Grobman-Hartman)**.** *Consider a vector field containing a hyperbolic equilibrium x_0. Then, this equilibrium has a neighborhood, in which the phase portrait is homeomorphic to that of the locally linearized system.*

Thus, for hyperbolic equilibria, we can still distinguish between foci, nodes and saddles based on the eigenvalues of the Jacobian matrix, which are often referred to as just the eigenvalues of the equilibrium.

In the case of a saddle, we introduce some useful terminology. Consider a linear vector field containing an equilibrium x_0 of saddle type. Thus, this equilibrium has a pair of real eigenvalues of opposing sign which we denote $\lambda_s < 0 < \lambda_u$. Along the eigenvectors

associated with these eigenvalues, solutions either move directly towards the saddle (for λ_s) or away from it (for λ_u). This explains the choice of notation s for *stable* and u for *unstable*. Thus, every saddle has associated with it two orbits converging to it when $t \to \infty$ and two orbits which converge to it when $t \to -\infty$. These orbits are sometimes referred to as ***separatrices***.

In a general (not necessarily linear) setting, the role of the eigenvectors is played by the ***stable manifold*** and ***unstable manifold*** of x_0 which are the sets

$$W^s(x_0) := \{x \in \mathbb{R}^2 : \varphi^t(x) \to x_0 \text{ as } t \to \infty\}$$
$$W^u(x_0) := \{x \in \mathbb{R}^2 : \varphi^t(x) \to x_0 \text{ as } t \to -\infty\}$$

where again, both manifolds of x_0 consist of two separatrices.

2.3 Cycles

Consider a solution $\gamma(t)$ of (2.1) for which there exists a minimal $T > 0$ such that

$$\gamma(t + T) = \gamma(t)$$

for all $t \in \mathbb{R}$. Such a solution is said to be ***periodic*** with period T. The orbit of a periodic solution is referred to as a ***cycle***.

Let x_0 be a point on a cycle. Because the vector field containing this cycle is smooth, we can introduce a ***cross-section*** Σ at x_0, which is a line segment orthogonal to the cycle. On this cross-section we may define a smooth coordinate ξ, where the point $\xi = 0$ coincides with x_0.

Note that the periodic solution through x_0 returns to Σ after time T. Again by smoothness, solutions starting at a point $x \in \Sigma$ close to x_0 also return to Σ close to x_0 after completing a trajectory near the cycle. Thus, we obtain a locally defined and discrete smooth map $P : \Sigma \to \Sigma$ called the ***Poincaré map*** associated with the cycle. The cycle at $\xi = 0$ is a fixed point of the Poincaré map yielding $P(0) = 0$. In fact, any fixed point of the Poincaré map corresponds with a cycle.

From the discrete dynamics of the Poincaré maps we can study the behaviour of the smooth solutions near the cycle, a considerable simplification. The Jacobian matrix of P at $\xi = 0$ yields the best linear approximation of P at $\xi = 0$. The single eigenvalue of this matrix, also called the ***multiplier*** μ of the cycle provides sufficient information to study the behaviour of P. A cycle with $\mu \neq 1$ is called ***hyperbolic***. If $\mu < 1$, iteratively applying P to a point on Σ

will bring this point closer and closer to $\xi = 0$. Thus, any solution which moves through the cross-section will converge towards the cycle. If this is case the cycle is said to be ***stable***. Similarly, if $\mu > 1$, the cycle is unstable. If $\mu \neq 1$ the cycle is referred to as a ***limit cycle*** because it is the limiting set of some collections of solutions of (2.1) as time increases forwards or backwards. We conclude that the eigenvalues and thus the stability of the fixed points of P directly corresponds to the stability of the cycle.

2.4 Homoclinic connections

In linear vector fields, the stable and unstable manifolds of an equilibrium intersect only at the saddle itself. Theorem 2.1 asserts that in non-linear systems the system locally looks the same. However, globally the situation may be different. For example, it may be the case that one of the orbits approaching x_0 coincides with one of the orbits leaving x_0. Thus, there exists a solution $\gamma(t)$ such that

$$\lim_{t\to-\infty} \gamma(t) = \lim_{t\to\infty} \gamma(t) = x_0.$$

The orbit associated with this solutions is known as a ***homoclinic connection***. Depending on the position of the other separatrices a homoclinic connection can be either *small* or *big* (see Figure 2.1).

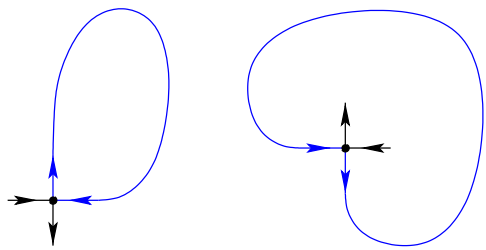

(a) (b)

Figure 2.1: Homoclinic connections to saddles: small (a) and big (b)

Now, we want to study the phase portrait near a homoclinic connection. Treatment of the big and small homoclinic connections is similar. Suppose therefore that at the saddle x_0 there exists a small homoclinic connection.

The following quantities will be of interest. Firstly we define the ***saddle quantity*** $\sigma = \lambda_s + \lambda_u$ which is a real number. Secondly

we define the ***saddle index*** $\lambda = -\lambda_s/\lambda_u$ which is a positive real number. Saddles with $\lambda > 1$ are sometimes called ***dissipative***, while saddles with $\lambda < 1$ are called ***non-dissipative***.

To begin, assume that our vector field is linear in the unit square, that is

$$\begin{cases} \dot{x}_1 &= \lambda_s x_1 \\ \dot{x}_2 &= \lambda_u x_2 \end{cases} \tag{2.2}$$

for $x = (x_1, x_2) \in [-1, 1] \times [-1, 1]$.

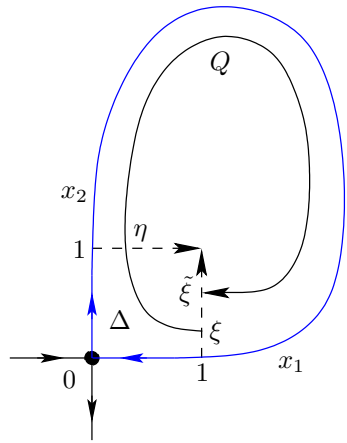

Figure 2.2: Singular and regular maps.

This allows us to compute explicitly the ***singular map*** along the orbits which pass near the saddle 0:

$$\eta = \Delta(\xi) = \xi^{\lambda}, \quad \xi > 0. \tag{2.3}$$

Indeed, the "flying time" τ from a point $(1, \xi)$ with $0 < \xi < 1$ to the point $(\eta, 1)$ along the orbit of (2.2) can be computed from the condition

$$1 = x_2(\tau) = \xi \mathrm{e}^{\lambda_u \tau},$$

so that

$$\tau = \frac{1}{\lambda_u} \ln\left(\frac{1}{\xi}\right) = -\frac{1}{\lambda_u} \ln \eta.$$

Substituting this expression into $\eta = \mathrm{e}^{\lambda_s \tau}$ gives (2.3). We can also set $\eta = 0$ for $\xi = 0$ by continuity.

The ***regular map***

$$\tilde{\xi} = Q(\eta) = \theta\eta + o(|\eta|), \tag{2.4}$$

is continuously-differentiable with its inverse, and $\theta > 0$ since the orbits do not cross.

The composition of the singular and the regular maps defines the **Poincaré map**:

$$\xi \mapsto \tilde{\xi} = Q(\Delta(\xi)) = \theta\xi^{\lambda} + o(\xi^{\lambda}). \tag{2.5}$$

This conclusion is valid in general, since there is a local invertible C^1 coordinate transformation that maps solutions of a nonlinear planar system near a saddle onto the solutions of (2.2), see [4] or [9] for a more geometric treatment. Thus, we have sketched a proof of the following result (see Figure 2.3).

Theorem 2.2. *If $\lambda > 1$ ($\lambda < 1$) then the homoclinic orbit Γ_0 is stable (unstable) from one side.* □

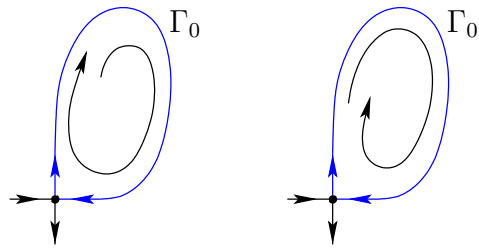

(a) $\sigma < 0$ (b) $\sigma > 0$

Figure 2.3: Stable and unstable small homoclinic orbits (loops).

Actually, there is a C^k linearizing transformation with any $k > 1$, if a finite number $N(k)$ of lower-order resonance conditions on the eigenvalues are not satisfied [14]. Thus the map (2.5) is generically as smooth as required for $\xi > 0$, provided the system (2.1) is sufficiently smooth. There is an alternative approach [13] that leads to the same map (2.5) but avoids a reduction to a linear system. In this approach, one first introduces new coordinates near the saddle, such that the system remains nonlinear but the stable and unstable manifolds locally coincide with the axes (and some other simplifications are done). Then by considering a boundary-value problem, one proves that the singular map near the saddle has the form

$$\Delta(\xi) = \xi^{\lambda} + o(\xi^{\lambda})$$

Composing this map with the regular global map (2.4), gives (2.5). The construction leads to a small finite loss of smoothness relative to that of (2.1).

2.5 Heteroclinic connections

Consider a vector field containing two saddles x_0 and x_1. In addition to solutions connecting a saddle to itself we may in this case also find solutions which connect one saddle to the other. Thus, there may exist a solution $\gamma(t)$ such that

$$\lim_{t\to-\infty} \gamma(t) = x_0 \quad \text{and} \quad \lim_{t\to\infty} \gamma(t) = x_1.$$

The orbit associated with such a solution curve is called a ***heteroclinic connection*** (see Figure 2.4).

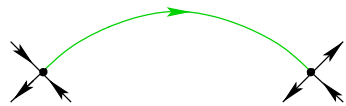

Figure 2.4: A heteroclinic connection between two saddles

3 Bifurcations and bifurcation diagrams

Having defined the necessary objects which might appear in a phase portrait, we come to the concept of bifurcation. Consider a system

$$\begin{cases} \dot{x}_1 = P(x_1, x_2, \alpha), \\ \dot{x}_2 = Q(x_1, x_2, \alpha), \end{cases} \tag{3.1}$$

where $\alpha \in \mathbb{R}^n$ is an n-dimensional ***parameter***. With the introduction of this parameter, (3.1) defines an n-dimensional ***family of vector fields***. Indeed, for any fixed choice of $\alpha \in \mathbb{R}^n$ we obtain a vector field as in (2.1).

Variation of the parameter results in different vector fields which in turn yield different phase portraits. However, we consider phase portraits to be equivalent whenever there exists a homeomorphism between them which preserves orbits, that is, takes orbits from one phase portraits to orbits of the other. If this is the case, we call the associated vector fields ***orbitally topologically equivalent***.

A vector field is said to be ***structurally stable*** if there exists a neighborhood of it in the space of all smooth vector fields, such

that all vector fields from this neighborhood are orbitally topologically equivalent. For parameter-dependent systems this implies the following: If a system for a given value of α is structurally stable, then there exists a neighborhood of α in the parameter space such that for all parameter values in this neighborhood the corresponding systems are orbitally topologically equivalent.

A ***bifurcation*** is then a qualitative change of the phase portrait under variation of the parameter which results in a phase portrait that is not topologically equivalent to the original one.

An overview of the bifurcational behaviour of a family of vector fields can be given in the form of a ***bifurcation diagram***. Such a diagram consists of a depiction of the parameter space (for example in the case of a two-dimensional parameter, a sketch of the parameter-plane) which is partitioned into sets corresponding to orbitally topologically equivalent vector fields. From this sketch one can see at a glance for which values of the parameters which bifurcation occurs. The diagram is completed when for every of these partitioning sets a representative phase portrait is supplied.

In practice, a bifurcation diagram is often produced by showing the set of points corresponding to structurally unstable vector fields. To this end, we have the following useful theorem.

Theorem 3.1 (Andronov-Pontryagin)**.** *A smooth vector field on a bounded region $D_0 \subset \mathbb{R}^2$ that is nowhere tangent to the boundary of this region is structurally stable if and only if*

- *It has a finite number of equilibria and limit cycles in D_0, and all of them are hyperbolic*;
- *There are no homoclinic or heteroclinic connections in D_0.*

From this theorem it follows that when producing a sketch of the bifurcation diagram, it is sufficient to investigate the violation of the above conditions.

To complete our preparation for the study of the bifurcational behaviour of heteroclinic contours in the plane we present and discuss all bifurcations which we will encounter during this process.

3.1 Homoclinic bifurcation

Consider now a system as in (3.1) with a parameter $\alpha \in \mathbb{R}$. Suppose that at $\alpha = 0$ this system has a homoclinic orbit Γ_0 to a hyperbolic saddle $x_0 = 0$ with saddle quantity $\sigma \neq 0$ (saddle index $\lambda \neq 1$). By the Implicit Function Theorem, there exists a smooth continuation

of this saddle for small $|\alpha|$, where we can place the origin of the coordinate system. Thus, $x_0 = 0$ will be a saddle equilibrium with eigenvalues $\lambda_s(\alpha) < 0 < \lambda_u(\alpha)$ for all sufficiently small $|\alpha|$ and with $\sigma(0) = \lambda_s(0) + \lambda_u(0) \neq 0$.

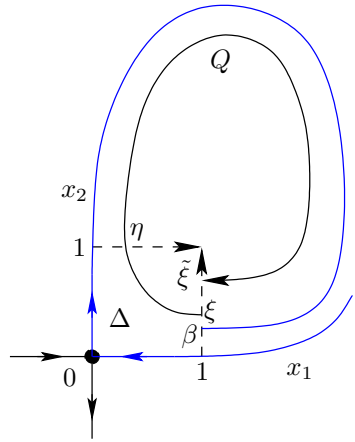

Figure 3.1: Poincaré map near saddle homoclinic bifurcation.

Similar to Section 2.4, first assume that (3.1) is linear in the square $[-1, 1] \times [-1, 1]$, i.e. can be written in the form

$$\begin{cases} \dot{x}_1 &= \lambda_s(\alpha)x_1, \\ \dot{x}_2 &= \lambda_u(\alpha)x_2. \end{cases} \tag{3.2}$$

The solutions of this system define a singular map near the saddle

$$\Delta : \xi \mapsto \eta = \xi^{-\frac{\lambda_s(\alpha)}{\lambda_u(\alpha)}} = \xi^{\lambda(\alpha)}$$

(see Figure 3.2). Outside of the square, the solutions of (3.1) define a regular map

$$Q : \eta \mapsto \tilde{\xi} = \beta(\alpha) + \theta(\alpha)\eta + o(|\eta|),$$

where $\theta(\alpha) > 0$, and $\beta(0) = 0$ since at $\alpha = 0$ there is a homoclinic orbit to the saddle at the origin. The function β describes the splitting of the saddle stable and unstable manifolds (separatrices) and is known as the ***splitting parameter***.

The composition $Q \circ \Delta$ gives the Poincaré map

$$\xi \mapsto \tilde{\xi} = \beta(\alpha) + \theta(\alpha)\xi^{\lambda(\alpha)} + \dots \ , \tag{3.3}$$

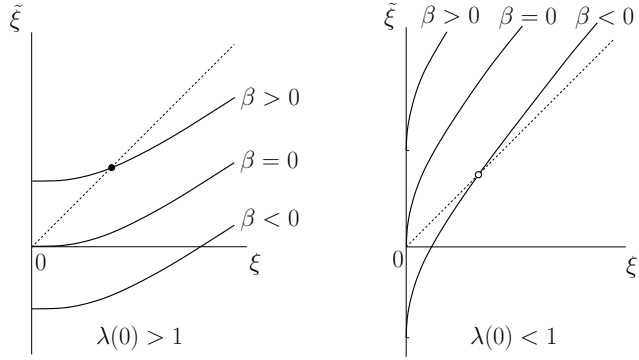

Figure 3.2: Bifurcation of fixed points of (3.3).

of which the fixed points are easy to analyze (see Figure 3.2). Since a fixed point corresponds to a cycle, we see that a unique cycle bifurcates from the saddle homoclinic orbit Γ_0 with $\lambda(0) \neq 1$ when β changes sign. The cycle is hyperbolic, and is stable for $\lambda(0) > 1$ and is unstable for $\lambda(0) < 1$. If follows that in order to analyse the bifurcation it is sufficient to study the **model map**

$$\xi \mapsto P(\xi) = \beta + \theta\xi^{\lambda}$$

with constant $\theta > 0$ and positive $\lambda \neq 1$.

As in Section 2.4, the above analysis is applicable in general. Thus, the following theorem is valid.

Theorem 3.2 (Andronov-Leontovich)**.** *Suppose that a smooth planar system*

$$\dot{x} = f(x, \alpha), \quad x \in \mathbb{R}^2, \ \alpha \in \mathbb{R},$$

has at $\alpha = 0$ a hyperbolic saddle with an orbit Γ_0 that is homoclinic to this saddle. Then, generically, a unique hyperbolic cycle bifurcates from Γ_0 for small $\alpha > 0$ or $\alpha < 0$, while the homoclinic orbit disappears:

(*i*) *If $\lambda(0) > 1$, the cycle is stable and the unstable separatrix of the saddle approaches it for $t \to +\infty$, see* Figure 3.3*;*

(*ii*) *If $\lambda(0) < 1$, the cycle is unstable and the stable separatrix of the saddle approaches it for $t \to -\infty$, see* Figure 3.4. □

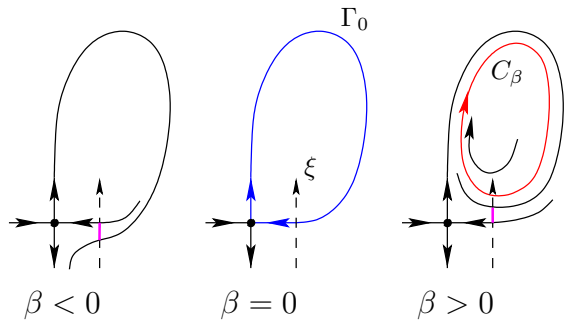

Figure 3.3: Saddle homoclinic bifurcation with $\lambda(0) > 1$: A stable cycle C_β bifurcates from Γ_0 while the separatrices exchange position.

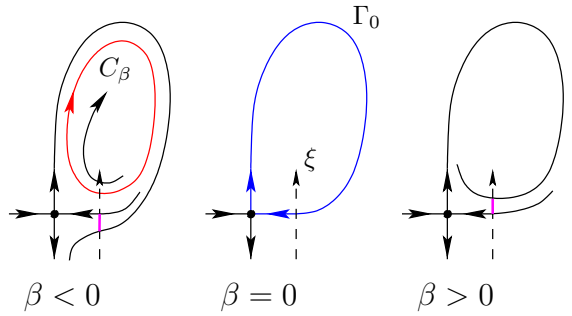

Figure 3.4: Saddle homoclinic bifurcation with $\lambda(0) < 1$: An unstable cycle C_β bifurcates from Γ_0 while the separatrices exchange position.

Note that the period of the cycle tends to infinity as α approaches zero. Indeed, the cycle passes closer and closer to the saddle, where the velocity $\dot{x}$ vanishes so that the passage takes more and more time.

The genericity conditions in Theorem 3.2 include $\lambda(0) \neq 1$ (i.e. $\sigma(0) \neq 0$), as well as a condition for the separatrices of the saddle to split under variation of α. This is guaranteed if β regularly changes sign at $\alpha = 0$, for which a sufficient condition is known.

3.1.1 Sandstede's Example

As a precursor to the final part of this thesis, we will now rederive the results of [12], which presents a derivation of a system containing a homoclinic connection. Perturbing this system will yield an example of a homoclinic bifurcation. In the final part of this thesis, we will adapt this technique to obtain more complicated example systems.

This technique is based on the idea of producing an algebraic set (or variety) which has a similar shape to a homoclinic connection. Once we have produced such a variety, we look for vector fields which are tangent to it. This tangency condition will then yield a system of polynomial equations from which we can derive two polynomials defining a vector field.

The Cartesian leaf (see Figure 3.5) is an algebraic variety which has a shape similar to a homoclinic connection.

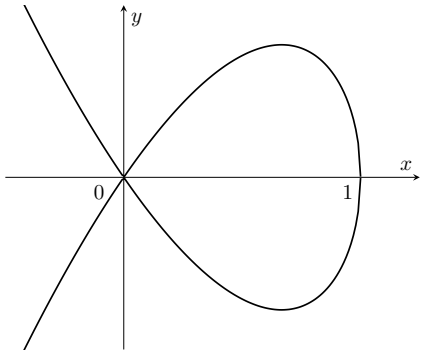

Figure 3.5: The Cartesian leaf

This variety is defined as the zero-set of the function $G : \mathbb{R}^2 \to \mathbb{R}$ defined by

$$G(x, y) = x^2(1 - x) - y^2.$$

Thus, we define the Cartesian leaf as $\Gamma := G^{-1}(0)$.

To find a polynomial vector field which is tangent to Γ we begin with a general polynomial vector field. It turns out that it is sufficient to consider polynomials of second order, yielding a system

$$f(x, y) = \begin{pmatrix} a_{00} + a_{10}x + a_{01}y + a_{20}x^2 + a_{11}xy + a_{02}y^2 \\ b_{00} + b_{10}x + b_{01}y + b_{20}x^2 + b_{11}xy + b_{02}y^2 \end{pmatrix}. \quad (3.4)$$

The condition of this vector field being tangent to Γ translates to the condition

$$\langle \nabla G(x,y), f(x,y) \rangle = 0 \quad \forall (x,y) \in \Gamma. \tag{3.5}$$

We are thus looking to find coefficients of $f(x,y)$ which render both polynomials $\langle \nabla G(x,y), f(x,y) \rangle$ and $G(x,y)$ identically zero simultaneously. From this we obtain a system of equations

$$\begin{cases} 2a_{00}x - 3a_{00}x^2 + 2a_{10}x^2 - 3a_{10}x^3 + 2a_{20}x^3 - 3a_{20}x^4 \\ -2b_{00}y + 2a_{01}xy - 2b_{10}xy - 3a_{01}x^2y + 2a_{11}x^2y \\ -2b_{20}x^2y - 3a_{11}x^3y - 2b_{01}y^2 + 2a_{02}xy^2 - 2b_{11}xy^2 \\ -3a_{02}x^2y^2 - 2b_{02}y^3 = 0 \\ x^2 - x^3 - y^2 = 0. \end{cases} \tag{3.6}$$

To solve this system we calculate its Gröbner basis using Mathematica. We use a suitable monomial ordering. This basis consists of several polynomials, including G and the following polynomial

$$\begin{aligned} P(x,y) = &-2a_{00}x + 2b_{00}y + (2b_{10} - 2a_{01})xy \\ &+ (3a_{00}a_{10} + a_{20})x^2 + (2b_{01} - 3a_{10} - a_{20})y^2 \\ &+ (2b_{11} - 2a_{02} - 3a_{20})xy^2 \\ &+ (3a_{01} + a_{11} + 2b_{20})x^2y \\ &+ (3a_{01} + a_{11} + 2b_{20})x^2y \\ &+ (2b_{02} - 3a_{11})y^3 + 3a_{02}x^2y^2 \end{aligned} \tag{3.7}$$

which must be identically equal to zero. Thus, every coefficient of P must equal zero which yields a number of constraints on the coefficients. Substituting these into the general polynomial vector field we obtain a system dependent on only three free coefficients, which we have renamed a, b and c for convenience. We find

$$f(x,y) = \begin{pmatrix} ax + by - ax^2 + cxy \\ bx + ay - \left(\frac{3}{2}b + \frac{1}{2}c\right)x^2 + \frac{3}{2}axy + \frac{3}{2}cy^2 \end{pmatrix}. \tag{3.8}$$

It is clear that this system has an equilibrium at the origin. To determine its type we calculate the Jacobian matrix of $f(x,y)$ which equals

$$J(x,y) = \begin{pmatrix} a - 2ax + cy & b + cx \\ b + \frac{3}{2}ay - (3b + c)x & a + \frac{3}{2}ax + 3cy \end{pmatrix}. \tag{3.9}$$

The Jacobian matrix at the equilibrium thus equals

$$J(0,0) = \begin{pmatrix} a & b \\ b & a \end{pmatrix} \tag{3.10}$$

which has eigenvalues $\lambda_1 = a+b$ and $\lambda_2 = a-b$. For the equilibrium to be a saddle, these eigenvalues must be nonzero and of opposite sign. This implies that $a^2 < b^2$.

Choosing $a = 1$, $b = -2$ and $c = 0$ we find that $\lambda_s = -1$, $\lambda_u = 3$ so the saddle index becomes $\lambda = -\lambda_s/\lambda_u = 1/3 < 1$. A phase portrait for this system with an unstable homoclinic orbit is presented in Figure 3.6.

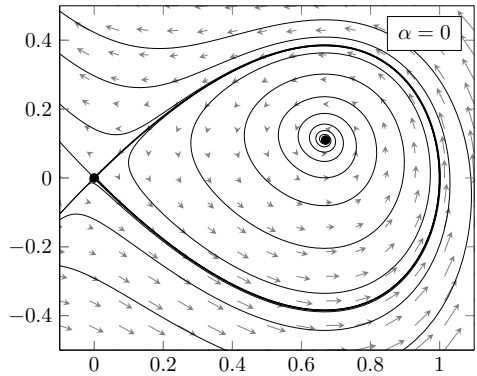

Figure 3.6: The phase portrait showing a homoclinic connection

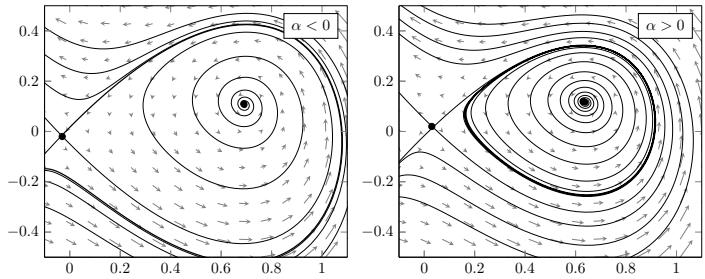

Figure 3.7: A homoclinic bifurcation generating an unstable cycle

Adding a constant perturbing parameter $\alpha \in \mathbb{R}$ to the second component of this system causes a homoclinic bifurcation generating an unstable cycle, see Figure 3.7.

3.2 Heteroclinic bifurcation

Just as in the case of a homoclinic connection, if under variation of a number of parameters a heteroclinic connection is broken, this implies a bifurcation.

An example of a system exhibiting this bifurcation is

$$\begin{cases} \dot{x} &= 1 - x^2 - \alpha xy, \\ \dot{y} &= xy + \alpha(1 - x^2) \end{cases} \tag{3.11}$$

with $\alpha \in \mathbb{R}$. Note that this system has two equilibria of saddle type at $x_0 = (-1, 0)$ and $x_1 = (1, 0)$. For $\alpha = 0$, this system has the x-axis as an invariant, that is, $\dot{y} = 0$ whenever $y = 0$. As the saddles are the only equilibria on the x-axis there must exist a solution $\gamma(t)$ such that

$$\lim_{t\to\infty} \gamma(t) = x_0 \quad \text{and} \quad \lim_{t\to-\infty} \gamma(t) = x_1$$

so $\gamma(t)$ is a heteroclinic connection.

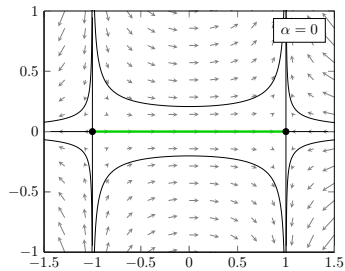

Figure 3.8: The phase portrait showing a heteroclinic connection

For $\alpha \neq 0$ the x-axis is no longer an invariant and the heteroclinic connection is broken.

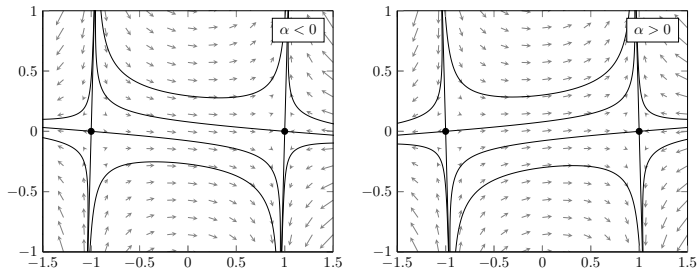

Figure 3.9: A heteroclinic bifurcation

3.3 Fold of cycles bifurcation

In order to understand the fold of cycles bifurcation we must first understand a general fold bifurcation of maps. Consider the one dimensional discrete system

$$\xi \mapsto \alpha + \xi + \xi^2 \tag{3.12}$$

depending on the parameter α. At $\alpha = 0$, this system has a fixed point at $\xi = 0$ which is non-hyperbolic and has multiplier $\mu = 1$. For $\alpha < 0$ this system has two fixed points at $\pm\sqrt{-\alpha}$ of which one is stable and the other is unstable. For $\alpha > 0$ the system has no fixed points.

We conclude that for increasing $\alpha < 0$ we start out with two fixed points of different stability which both move towards $x = 0$ when α goes to 0. At $\alpha = 0$, these fixed points collide and momentarily form a single fixed point which is stable from one side and unstable from the other. Such a fixed point is said to be ***semi-stable***. Increasing α even more destroys this semi-stable point leaving a system without fixed points. This bifurcation involving the collision and destruction of two fixed points of different stability is known as a ***fold bifurcation***.

It turns out that under some general non-degeneracy conditions (see [9] for details) any smooth map containing at $\alpha = 0$ a fixed point with $\mu = 1$ is topologically equivalent to (3.12). Actually, one can show that there exists a smooth transformation of coordinates and parameters reducing the map to (3.12) plus higher-order terms, which do not change the local orbit structure.

Now consider a system of the form (2.1) containing a limit cycle which corresponds to a fixed point ξ_0 with multiplier $\mu = 1$ of

the Poincaré map P, defined on a one-dimensional cross-section Σ. From the discussion relating the stability of the fixed points of P to the stability of the cycles we conclude that this cycle is also semi-stable, so stable from one side while unstable from the other.

By the above discussion, this fixed point ξ_0 with multiplier $\mu = 1$ is generically the result of a collision of two fixed points of opposing stability. Because these fixed points are fixed points of the Poincaré map P, they coincide with limit cycles of (2.1) and the stability of these cycles is implied by the stability of the fixed points, that is, one cycle is stable while the other cycle is unstable.

Thus the ***fold of cycles bifurcation*** can be seen as the result of a fold bifurcation on the cross-section Σ and can be described as the collision of two limit cycles of opposite stability type, resulting in the birth of a critical semi-stable limit cycle which is non-hyperbolic and structurally unstable.

The following system exhibiting a subcritical degenerate Hopf bifurcation also undergoes a fold of cycles bifurcation.

$$\begin{cases} \dot{x} = (\alpha - \frac{1}{4})x - y + x(x^2 + y^2) - x(x^2 + y^2)^2, \\ \dot{y} = x + (\alpha - \frac{1}{4})y + y(x^2 + y^2) - y(x^2 + y^2)^2 \end{cases} \tag{3.13}$$

As seen from Figure 3.10, for $\alpha > 0$, the system contains a stable limit cycle enclosing an unstable one. These limits cycles collide at $\alpha = 0$ forming a semi-stable cycle which is unstable from the inside but stable from the outside. For $\alpha < 0$, this limit cycle is destroyed and no cycles remain.

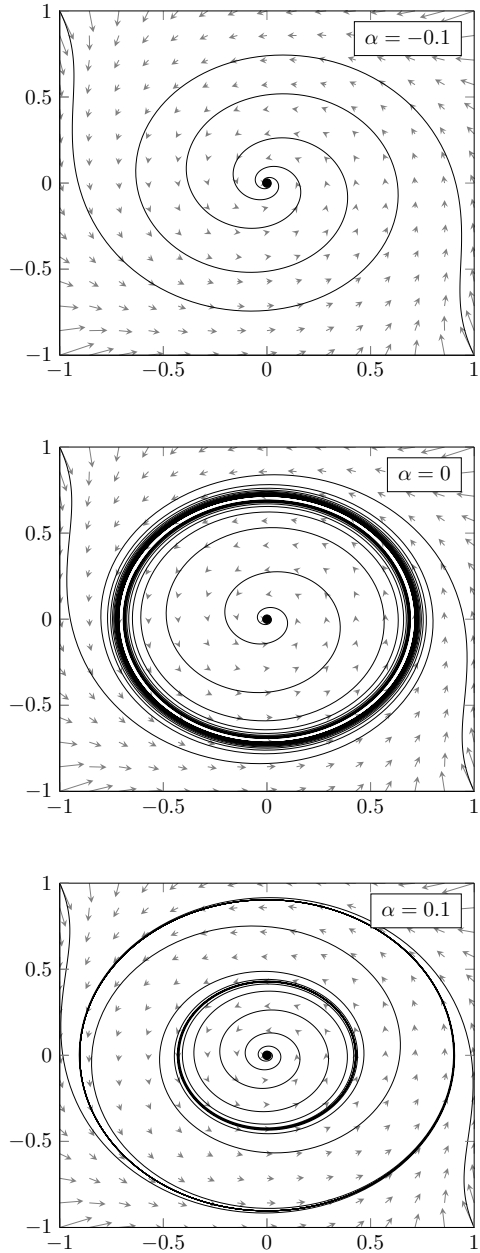

Figure 3.10: Phase portraits showing a fold of cycles bifurcation

3.4 Flashing heteroclinic connections

The last type of bifurcation under consideration is also the most exotic. In fact, the appearance of this bifurcation is one of the most important reasons to study bifurcations of heteroclinic contours at all, as it results in a bifurcation diagram which is surprisingly complex for a system which is only planar.

As noted in the introduction, this bifurcation was discovered in 1981 by I.P. Malta and J. Palis in [10], see also [13]. The flashing of heteroclinic connections refers to the generation of an infinite series of heteroclinic connections between two saddles which make an increasing number of turns around one of the saddles before reaching the other.

The situation in which this bifurcation was first discovered was at a one-parameter bifurcation of a non-hyperbolic limit cycle. Of the two saddles involved in this bifurcation, one is located inside the limit cycle while the other is located on the outside[1]. The non-hyperbolic limit cycle serves as the limit set of a solution leaving the outside saddle for increasing t while simultaneously it is approached for decreasing t by a solution approaching the other saddle for increasing t. Thus, there are solutions winding around the cycle from both the outside and inside.

The following theorem shows that when this limit cycle is destroyed, an infinite series of heteroclinic connections is generated which wind around the inside saddle an increasing number of times (see Figure 3.14).

In the theorem we consider the parameter $\alpha \in \mathbb{R}$ involved in the fold of cycles bifurcation. Thus, for $\alpha = 0$ there exists a semi-stable limit cycle as described above and for $\alpha > 0$ this cycle is destroyed.

Theorem 3.3. *Consider a vector field containing two saddles and a semi-stable limit cycle as described above. Then there exists a sequence $(\alpha_n)_{n\in\mathbb{N}}$ with $\alpha_n > 0$ for all $n \in \mathbb{N}$ and $\alpha_n \to 0$ such that for every $n \in \mathbb{N}$, the vector field corresponding to the parameter value α_n contains a heteroclinic connection making more turns around the inner saddle then the previous one.*

Proof. For $\alpha = 0$, the vector field contains a semi-stable limit cycle which separates the saddles L and M. On this cycle we define a cross-section Σ on which we define a coordinate x directed outwards (see Figure 3.11). Suppose that the limit cycle and its cross-section

[1] Of course, more equilibria must be encircled by the cycle.

intersect at $x = 0$. The orbit moving towards the saddle L reaches the cross-section at $x_1 < 0$ and the orbit leaving from M at $x_2 > 0$.

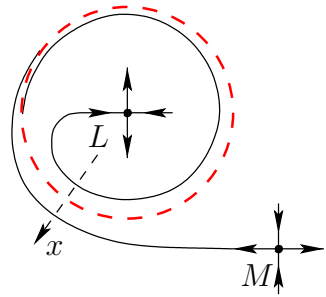

Figure 3.11: Placing a cross-section on the cycle

When we pick $\alpha > 0$ and study the vector field still furnished with the cross-section Σ, we see that we get parameter dependent values of $x_1(\alpha) < 0 < x_2(\alpha)$ and that the semi-stable limit cycle is destroyed. Thus, the parameter dependent Poincaré map P_α has no fixed points. Therefore, we have that $P_\alpha(x) < x$ so after enough iterations of the Poincaré map we will find $n \in \mathbb{N}$ and $m \in \mathbb{N}$ such that $P_\alpha^{(-n)}(x_1(\alpha)) > 0$ and $P_\alpha^{(m)}(x_2(\alpha)) < 0$.

In contrast to this, we always have that $P_\alpha(x_1(0)) < 0$ and $P_\alpha(x_2(0)) > 0$. Thus, assuming that $n \geq m$, and letting $\alpha \to 0$ we will find α_n such that $P_{\alpha_n}^{(-n)}(x_1(\alpha_n)) = P_{\alpha_n}^{(n)}(x_2(\alpha_n)) = 0$ which coincides with a heteroclinic connection. □

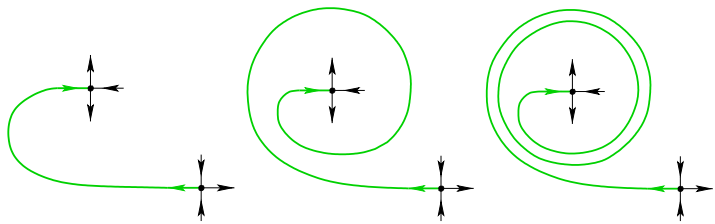

(a) No turns (b) One turn (c) Two turns

Figure 3.12: Heteroclinic connections making an increasing number of turns

The occurrence of flashing heteroclinic connections is not limited to situations involving a fold of cycles bifurcation. They may

also appear in a similar situation involving the bifurcation of a homoclinic connection. More specifically, we consider the situation in which there exist two saddles and a homoclinic connection at one of the saddles. The other saddle is located inside this saddle. We consider a system depending on the splitting parameter β of the homoclinic connection. Suppose the saddle at which the homoclinic connection exists has saddle index smaller than one, so for $\beta > 0$ the homoclinic connection is broken and no limit cycle is generated.

Theorem 3.4. *Consider a vector field containing two saddles and a homoclinic connection as described above. Then there exists a sequence $(\beta_n)_{n\in\mathbb{N}}$ with $\beta_n > 0$ for all $n \in \mathbb{N}$ and $\beta_n \to 0$ such that for every $n \in \mathbb{N}$, the vector field corresponding to the parameter values β_n contains a heteroclinic connection making more turns around the inner saddle then the previous one.*

Proof. The vector field for $\beta = 0$ contains a homoclinic connection at M and L lies on the inside of this connection. The solutions leaving L have the homoclinic connection as its limit set. On this connection we define a cross-section Σ on which we define a coordinate x directed inwards (see Figure 3.13). Suppose that the homoclinic connection (that is, the solution leaving and approaching M) and its cross-section intersect at $x = 0$ and that the solution leaving the saddle L reaches the cross-section at $x_1 > 0$.

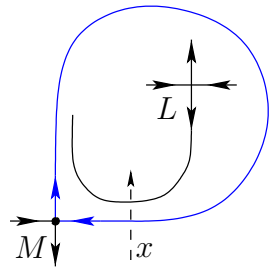

Figure 3.13: Placing a cross-section on the homoclinic connection

When we pick $\beta > 0$ and study the vector field, still furnished with the cross-section Σ, we see that we get parameter dependent values of $x_1(\beta) > 0$ and that the homoclinic connection is destroyed. Moreover, the parameter dependent Poincaré map P_β has no fixed points. Therefore, we have that $P_\beta(x) < x$ so after

enough iterations of the Poincaré map we will find $n \in \mathbb{N}$ such that $P_\beta^{(n)}(x_1(\beta)) < 0$.

In contrast to this, we always have that $P_\beta(x_1(0)) > 0$. Thus, letting $\beta \to 0$ we will find β_n such that $P_{\beta_n}^{(n)}(x_1(\beta_n)) = 0$ which coincides with a heteroclinic connection. □

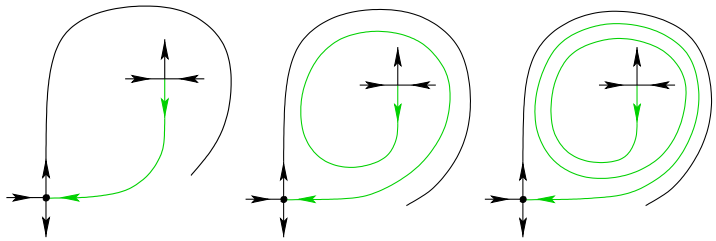

(a) No turns (b) One turn (c) Two turns

Figure 3.14: Heteroclinic connections making an increasing number of turns

Part III
Bifurcations of heteroclinic contours

We are now ready to start our investigation of the bifurcations of planar heteroclinic contours. We begin by giving a proper definition of a system containing a heteroclinic contour and distinguish several cases.

Firstly, a distinction will be made between monodromic and non-monodromic contours. In both cases we introduce two splitting parameters which describe how the heteroclinic connections involved in the contour are broken. At this stage, we are ready to introduce a number of model maps which will serve as the primary tools used in this part of the thesis. Then, a further distinction is made based on the saddle indices of the involved saddles. In each case, two subcases are to be considered, yielding a total of four different cases.

Each case is treated separately. In each case our primary objective will be to produce a complete sketch of the bifurcation diagram. In accordance with Theorem 3.1 this is done by studying the appearance of homoclinic connections, hyperbolic and non-hyperbolic limit cycles and heteroclinic connections, in this order.

4 Heteroclinic contours

Consider a smooth vector field as in (2.1) and assume this vector field contains two equilibria of saddle type which we label L and M. Let λ and μ be the saddle indices of L and M respectively. Also suppose that this vector field has solutions $\gamma_1(t)$ satisfying

$$\lim_{t\to-\infty}\gamma_1(t) = L \quad \text{and} \quad \lim_{t\to\infty}\gamma_1(t) = M$$

and $\gamma_2(t)$ satisfying

$$\lim_{t\to-\infty}\gamma_1(t) = M \quad \text{and} \quad \lim_{t\to\infty}\gamma_1(t) = L.$$

We see that the orbits of $\gamma_1(t)$ and $\gamma_2(t)$ are heteroclinic connections between L and M in opposing directions. Together with the saddles they form a ***heteroclinic contour***.

Depending on the position of the stable and unstable manifolds of L and M there are two distinct types of heteroclinic contours called ***monodromic*** and ***non-monodromic***, see Figure 4.1.

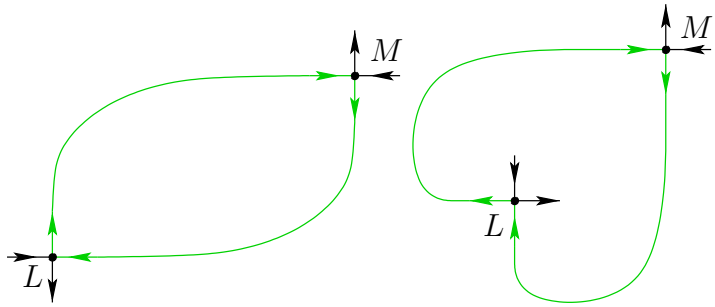

(a) Monodromic (b) Non-monodromic

Figure 4.1: The two types of heteroclinic contours

To understand this choice of terminology, note that the monodromic contour may be approached as a limit set by solutions inside the contour. It is also possible to contain all stable and unstable manifolds inside the contour, in which case the contour may be approached as a limit set for solutions outside the contour. This case is also referred to as monodromic and is treated similarly. In the non-monodromic case, the contour can not be approached as a limit set, neither from the inside nor the outside.

4.1 Model maps

4.1.1 Monodromic

As in Section 2.4 we introduce a number of model maps to study the heteroclinic contours. We begin with the monodromic case. As we have seen before, we define a number of cross-sections on which the model maps will be defined (see Figure 4.2).

In a neighborhood of L, we introduce two cross-sections, Σ_L and Π_L, on the incoming and outgoing heteroclinic connection respectively. On these cross sections, we introduce coordinates ξ_L and η_L, again respectively. We define these coordinates in such a way that the points $\xi_L = 0$ and $\eta_L = 0$ coincide with the points on the intersection of the stable and unstable manifolds and the corresponding cross-section, and such that positive values of the coordinates correspond with points inside the heteroclinic contour.

Analogously, in a neighborhood U_M of M, we introduce cross-sections Σ_M and Π_M furnished with coordinates ξ_M and η_M with analogous properties.

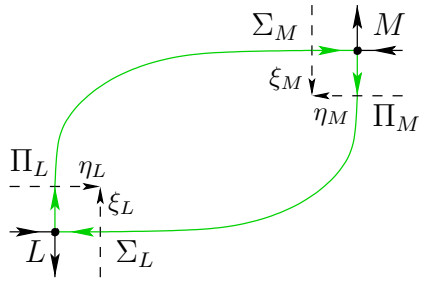

Figure 4.2: The monodromic contour with all cross-sections and coordinates

Using the cross-sections, we define the splitting parameters β_1 and β_2 which measure the splitting of the heteroclinic connection along Σ_L and Σ_M respectively.

As in Section 2.4 we may now define exact singular maps $\Delta_L : \Sigma_L \to \Pi_L$ and $\Delta_M : \Sigma_M \to \Pi_M$ by

$$\Delta_L(\xi_L) = \xi_L^\lambda \quad \text{and} \quad \Delta_M(\xi_M) = \xi_M^\mu$$

near the saddles and truncated regular maps $Q : \Pi_L \to \Sigma_M$ and $R : \Pi_M \to \Sigma_L$ by

$$Q(\eta_L) = \beta_2 + \theta_1 \eta_L \quad \text{and} \quad R(\eta_M) = \beta_1 + \theta_2 \eta_M$$

near the heteroclinic connections where θ_1 and θ_2 are positive constants. By composing these maps we arrive at the truncated Poincaré map $P : \Sigma_L \to \Sigma_L$ which becomes

$$\begin{aligned} P(\xi_L) &= (R \circ \Delta_M \circ Q \circ \Delta_L)(\xi_L) \\ &= \beta_1 + \theta_2(\beta_2 + \theta_1 \xi_L^\lambda)^\mu. \end{aligned} \tag{4.1}$$

4.1.2 Non-monodromic

The construction of the model maps in the non-monodromic case is virtually the same as in the monodromic case. However, to obtain a singular map describing the behaviour of solution near the saddle, the cross-sections at L must be oriented in the other direction to

allow solutions to pass near the saddles on the positive side of the cross-sections.

The new configuration of the cross sections is pictured in Figure 4.3.

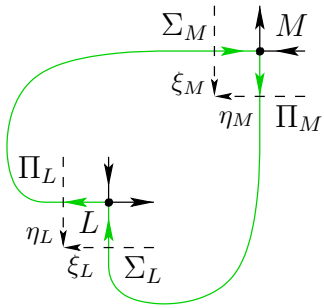

Figure 4.3: The non-monodromic contour with all cross-sections and coordinates

Consequently, the splitting parameters at L are now also measured in the other direction. This change allows us to express the exact singular maps $\Delta_L : \Sigma_L \to \Pi_L$ and $\Delta_M : \Sigma_M \to \Pi_M$ in exactly the same way as before, thus as

$$\Delta_L(\xi_L) = \xi_L^\lambda \quad \text{and} \quad \Delta_M(\xi_M) = \xi_M^\mu.$$

However this change does have an effect on the truncated regular maps $Q : \Pi_L \to \Sigma_M$ and $R : \Pi_M \to \Sigma_L$ which in this case become

$$Q(\eta_L) = \beta_2 - \theta_1\eta_\lambda \quad \text{and} \quad R(\eta_M) = \beta_1 - \theta_2\eta_M.$$

Thus, in the non-monodromic case we obtain the truncated Poincaré map $P : \Sigma_L \to \Sigma_L$ as

$$P(\xi_L) = \beta_1 - \theta_2(\beta_2 - \theta_1\xi_L^\lambda)^\mu. \tag{4.2}$$

Note that in terms of the model maps we can change between the monodromic and non-monodromic cases through the transformation $(\theta_1, \theta_2) \mapsto (-\theta_1, -\theta_2)$.

4.2 Dissipativity of the saddles

We note that in both cases the Poincaré map depends strongly on the values of λ, μ and also $\lambda\mu$. Especially, it is important whether

these quantities are smaller or larger than 1. Recall that saddles with index greater than one are called dissipative. In principle, the following subcases are possible.

1	$\lambda < 1$	$\mu > 1$	$\lambda\mu < 1$
2	$\lambda < 1$	$\mu > 1$	$\lambda\mu > 1$
3	$\lambda > 1$	$\mu < 1$	$\lambda\mu > 1$
4	$\lambda > 1$	$\mu < 1$	$\lambda\mu < 1$
5	$\lambda > 1$	$\mu > 1$	$\lambda\mu > 1$
6	$\lambda < 1$	$\mu < 1$	$\lambda\mu < 1$

However, reversing time and interchanging the roles of L and M, we see that there are only two essentially different subcases to consider. More specifically, reversing time, we see that 1 goes to 3 and 5 to 6. When changing the roles of L and M, 1 goes to 4 and 2 to 3. Thus if we study only the subcases 1 and 6, the results for all others follow immediately. To conclude, we consider only subcases $\lambda < 1$, $\mu < 1$ and $\lambda < 1$, $\mu > 1$ with $\lambda\mu < 1$ in both of them.

5 The monodromic case

Having made the necessary distinctions we are ready to treat both subcases of the monodromic case. As stated at the beginning of this part we proceed in the following way. We begin by studying the emergence of homoclinic connections. Then we investigate limit cycles and their bifurcations. Lastly, we look at heteroclinic connections. From these results we will then be able to sketch the bifurcation diagram.

We will find that in both subcases there exist two curves in the parameter plane corresponding to homoclinic connections at L and M. Together with the origin, these curves divide the parameter plane in two sectors.

In the first subcase ($\lambda < 1$ and $\mu < 1$) we find that for parameter values in one of these sectors there are no limit cycles present. Then, moving to the other sector, an unstable limit cycle is generated as a result of the breaking up of either one of the homoclinic connections.

In the second subcase ($\lambda < 1$ and $\mu > 1$), an unstable limit cycle is again generated when the homoclinic connection at L is broken. Additionally, if we vary the parameters further such that the homoclinic connection at M (corresponding now to saddle index $\mu > 1$)

is broken, a stable cycle is generated enclosing the original unstable cycle. Eventually these cycles collide and momentarily form a semi-stable limit cycle at a fold of cycles bifurcation. In the remaining regions, no limit cycles are present.

The results in this section are originally due to [11]. However, we use a different approach similar to that in [7].

5.1 Homoclinic connections

From the geometry of the monodromic contour (see Figure 5.1) it is readily seen that a homoclinic connection at L may only arise whenever $\beta_1 < 0$ and $\beta_2 > 0$.

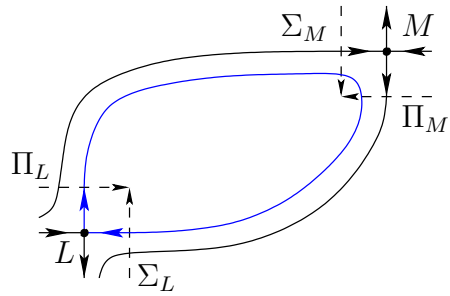

Figure 5.1: The appearance of a homoclinic connection at L

Moreover, a homoclinic connection at L coincides with a solution of the equation

$$(R \circ \Delta_M \circ Q)(0) = \beta_1 + \theta_2 \beta_2^{\mu} = 0 \tag{5.1}$$

which we can rewrite into the expression

$$\beta_2 = \left(-\frac{\beta_1}{\theta_2} \right)^{\frac{1}{\mu}}$$

for β_2 in terms of β_1.

A similar discussion can be had for the emergence of homoclinic connections at M. Firstly, we note that such connections may only arise whenever $\beta_1 > 0$ and $\beta_2 < 0$. At M, a homoclinic connection coincides with a solution of the equation

$$(Q \circ \Delta_L \circ R)(0) = \beta_2 + \theta_1 \beta_1^{\lambda} = 0 \tag{5.2}$$

which we can rewrite into the expression

$$\beta_2 = -\theta_1 \beta_1^{\lambda}$$

for β_2 in terms of β_1.

Thus, we find that there are two curves in the parameter plane corresponding to homoclinic connections at L and M. We label these curves P_L and P_M respectively. Sketching these curves in the parameter-plane is our first step in sketching the bifurcation diagram. Depending on the two different subcases, we obtain different curves, see Figure 5.2.

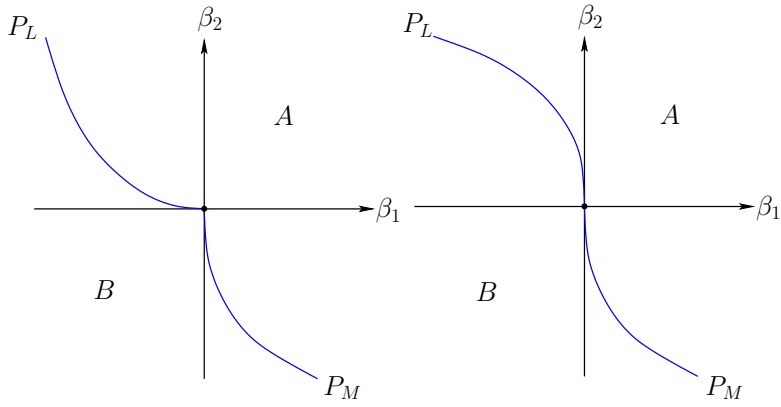

(a) $\lambda < 1$ and $\mu < 1$ (b) $\lambda < 1$ and $\mu > 1$

Figure 5.2: The emergence of homoclinic connections in the parameter-plane

For ease of reference, we label the two sectors of the parameter-plane delineated by P_L and P_M as A and B.

5.2 Limit cycles

As we have seen in Section 2.3, limit cycles correspond to fixed points of the Poincaré map, in this case (4.1). Thus we are looking for solutions ξ_L of

$$\beta_1 + \theta_2(\beta_2 + \theta_1 \xi_L^{\lambda})^{\mu} = \xi_L. \tag{5.3}$$

This equation may be rewritten as

$$\beta_2 + \theta_1 \xi_L^{\lambda} = \left(\frac{\xi_L - \beta_1}{\theta_2} \right)^{\frac{1}{\mu}}.$$

To look for solutions of this equation we consider the left- and right-hand side separately. To this end, we define functions f and g by

$$f(\xi_L) = \beta_2 + \theta_1 \xi_L^\lambda \quad \text{and} \quad g(\xi_L) = \left(\frac{\xi_L - \beta_1}{\theta_2} \right)^{\frac{1}{\mu}}$$

which allows us to rewrite (5.3) as $f(\xi_L) = g(\xi_L)$.

To study solutions of this equation we will also need the derivatives of f and g which we find to be

$$f'(\xi_L) = \lambda \theta_1 \xi_L^{\lambda - 1} \quad \text{and} \quad g'(\xi_L) = \frac{1}{\mu \theta_2} \left(\frac{\xi_L - \beta_1}{\theta_2} \right)^{\frac{1}{\mu} - 1}.$$

Additionally, the maps f and g have an intuitive geometric interpretation which will relate them to the generation of homoclinic connections. In terms of the model maps, we can see that $f = Q \circ \Delta_L$ while $g = (R \circ \Delta_M)^{-1}$. Thus, both can be seen as maps from Σ_L to Σ_M. This point of view makes it clear that the solution $f(0) = g(0)$ coincides with a homoclinic connection at L, while a solution $\xi_L \neq 0$ satisfying $f(\xi_L) = g(\xi_L) = 0$ coincides with a homoclinic connection at M.

Furthermore, we have expressions for

$$f(0) = \beta_2 \quad \text{and} \quad g(0) = \left(-\frac{\beta_1}{\theta_2} \right)^{\frac{1}{\mu}}$$

and we can find solutions to $f(\xi_L^f) = 0$ and $g(\xi_L^g) = 0$, namely

$$\xi_L^f = \left(-\frac{\beta_2}{\theta_1} \right)^{\frac{1}{\lambda}} \quad \text{and} \quad \xi_L^g = \beta_1.$$

From this point on we must treat both subcases separately.

5.2.1 The first subcase

As in this case both $\lambda < 1$ and $\mu < 1$, the maps f and g have the limiting properties

$$\lim_{\xi_L \downarrow 0} f(\xi_L) = \beta_2 \quad \text{and} \quad \lim_{\xi_L \downarrow 0} f'(\xi_L) = \infty$$

while

$$\lim_{\xi_L \downarrow \beta_1} g(\xi_L) = 0 \quad \text{and} \quad \lim_{\xi_L \downarrow \beta_1} g'(\xi_L) = 0$$

which tells us that f is convex upwards while g is convex downwards.

A useful observation is that in this case, for arbitrarily small values of the parameters, there will be no small values of ξ_L where f and g have equal derivative. To see this, suppose that $f'(\xi_L) = g'(\xi_L)$ so

$$\lambda\theta_1\xi_L^{\lambda-1} = \frac{1}{\mu\theta_2}\left(\frac{\xi_L - \beta_1}{\theta_2}\right)^{\frac{1}{\mu}-1}.$$

We may rewrite this into the expression

$$\beta_1 = \xi_L - \theta_2(\lambda\mu\theta_1\theta_2)^{\frac{\mu}{1-\mu}}\xi_L^{\frac{\mu(\lambda-1)}{1-\mu}}.$$

Noting that $\frac{\mu(\lambda-1)}{1-\mu} < 0$ by our assumption on λ and μ we see that $\lim_{\xi_L \downarrow 0} \beta_1(\xi_L) = -\infty$. Thus, letting ξ_L as well as the parameters go to zero, f and g can not have the same derivative at ξ_L.

This result locally precludes tangency of f and g and also implies that locally there may be at most one intersection of f and g. As, by Rolle's theorem, between any two intersections of f and g we can find a point where they have equal derivative.

Suppose that we choose a pair of parameters from sector A. For $\beta_1 < 0$ this point lies above P_L and for $\beta_1 > 0$ this point lies above P_M.

Suppose $\beta_1 < 0$, we then find that

$$\beta_2 > \left(-\frac{\beta_1}{\theta_2}\right) \quad \text{so} \quad f(0) > g(0)$$

and $\beta_2 > 0$. This, together with their limiting properties, implies that f and g do not intersect for arbitrarily small values of β_1 and β_2 as can be seen from Figure 5.3a.

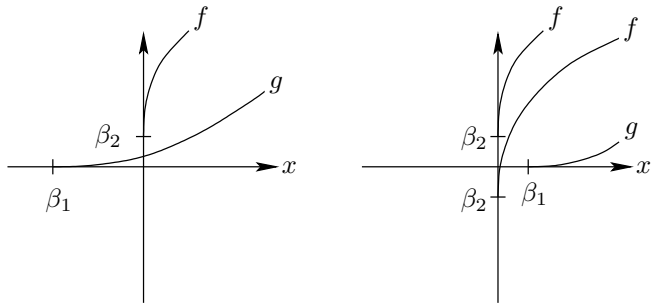

(a) $\beta_1 < 0$ (b) $\beta_1 > 0$

Figure 5.3: Possible configurations of f and g for parameters from sector A

In the case that $\beta_1 > 0$ we find that

$$\left(-\frac{\beta_2}{\theta_1}\right)^{\frac{1}{\lambda}} < \beta_1 \quad \text{so} \quad \xi_L^f < \xi_L^g$$

and $\beta_2 < 0$ or that $\beta_2 > 0$. This again implies that f and g do not intersect for arbitrarily small values of β_1 and β_2 as can be seen from Figure 5.3b.

Thus, for parameter values in sector A there are no limit cycles. Moving on to sector B, we have for $\beta_1 < 0$ that we are below P_L and for $\beta_2 > 0$ that we are above P_M.

Suppose then that $\beta_1 < 0$. It then holds similarly that $f(0) < g(0)$ while $\beta_2 < 0$ or $\beta_2 > 0$. In this case we do find that f and g intersect for arbitrarily small values of β_1 and β_2, as can be seen from Figure 5.4a.

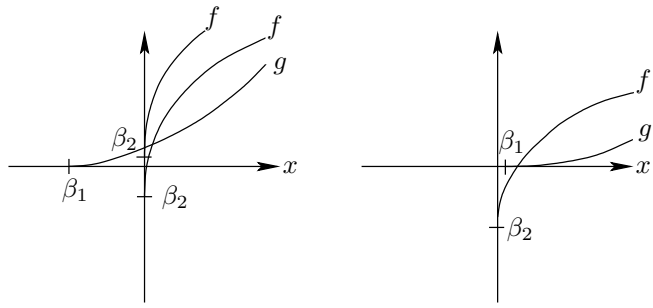

(a) $\beta_1 < 0$ (b) $\beta_1 > 0$

Figure 5.4: Possible configurations of f and g for parameters from sector B

In the remaining case that $\beta_1 > 0$ we have again similarly that $\xi_L^f > \xi_L^g$ while $\beta_2 < 0$. Again, we find that f and g intersect for arbitrarily small values of β_1 and β_2, as can be seen from Figure 5.4b.

Thus, for parameter values in sector B there is a single limit cycle.

5.2.2 The second subcase

It now holds that $\lambda < 1$ while $\mu > 1$ which implies that

$$\lim_{\xi_L \downarrow 0} f(\xi_L) = \beta_2 \quad \text{and} \quad \lim_{\xi_L \downarrow 0} f'(\xi_L) = \infty$$

while

$$\lim_{\xi_L \downarrow \beta_1} g(\xi_L) = 0 \quad \text{and} \quad \lim_{\xi_L \downarrow \beta_1} g'(\xi_L) = \infty$$

so now both f and g are convex upward. Note that the standing assumption $\lambda\mu < 1$ implies that $\lambda < \frac{1}{\mu}$. Thus for small values of the parameters we may expect the graph of f to be steeper than that of g.

We repeat the arguments from the first subcase which now yield different results. Again assume that we choose a pair of parameters from sector A. When $\beta_1 < 0$ we again find that $f(0) > g(0)$ and that $\beta_2 > 0$. Once more, this implies that there is no intersection of f and g as is clear from Figure 5.4b.

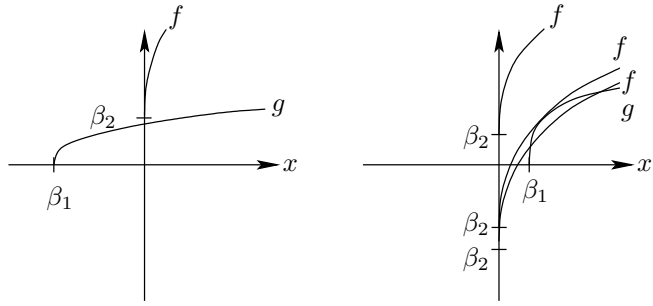

(a) $\beta_1 < 0$ (b) $\beta_1 > 0$

Figure 5.5: Possible configurations of f and g for parameters from sector A

When $\beta_1 > 0$ the situation is different. When $\beta_2 > 0$ there are still no intersections but when $\beta_2 < 0$ it must again hold that $\xi_L^f < \xi_L^g$ in which case there now may be either no, one or two intersection and thus limit cycles as illustrated in Figure 5.5b. We see that there exists one limit cycle if and only if f and g are tangent. This situation is structurally unstable. Variation of the parameters immediately results into either one or two limit cycles. We recognize that there thus occurs a fold of cycles bifurcation.

Moving on to sector B, and assuming that $\beta_1 < 0$ we again obtain that $f(0) < g(0)$ and that $\beta_2 < 0$ or $\beta_2 > 0$. In this case we find that there is one intersection of f and g as is seen in Figure 5.6a.

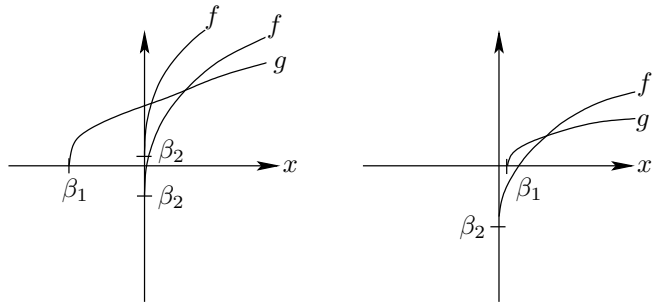

(a) $\beta_1 < 0$ (b) $\beta_1 > 0$

Figure 5.6: Possible configurations of f and g for parameters from sector B

The remaining case of $\beta_1 > 0$ implies that $\xi_L^f > \xi_L^g$ and that $\beta_2 < 0$ which also shows that there is one intersection, visible from Figure 5.6b.

In conclusion, for parameters in sector B there is again a single limit cycle.

5.2.3 Semi-stable cycle

The semi-stable which appears at a fold of cycles bifurcation requires some more attention. As vector fields containing such a cycle are structurally unstable, it is necessary to know for which values of the parameters they appear when sketching the bifurcation diagram.

As we have seen, a semi-stable limit cycle appears exactly when the graphs of f and g are tangent. This yields the conditions $f(\xi_L) = g(\xi_L)$ and $f'(\xi_L) = g'(\xi_L)$ yielding

$$\beta_2 + \theta_1 \xi_L^\lambda = \left(\frac{\xi_L - \beta_1}{\theta_2} \right)^{\frac{1}{\mu}}$$

and

$$\lambda \theta_1 \xi_L^{\lambda - 1} = \frac{1}{\mu \theta_2} \left(\frac{\xi_L - \beta_1}{\theta_2} \right)^{\frac{1}{\mu} - 1}.$$

In [11], the following expression for β_2 in terms of β_1 is derived using the above two conditions:

$$\beta_2 = -\theta_2 \beta_1^\lambda - (1 - \mu^\mu)(\lambda \mu \theta_1 \theta_2)^{\frac{1}{1-\mu}} \beta_1^{\frac{\lambda - 1}{1 - \mu}} \tag{5.4}$$

5.3 Heteroclinic connections

It is clear from the geometry of the monodromic case and the definition of the splitting parameters that heteroclinic connections are only possible when one of the parameters is zero. Thus, in the bifurcation diagram, the curves corresponding to heteroclinic connections are exactly the axes.

5.4 Sketching the bifurcation diagram

Summarising the results of both monodromic subcases, we may now sketch the bifurcation diagrams. As before, we denote the curves corresponding to homoclinic connections P_L and P_M. In the second subcase, we denote the curve in the parameter plane corresponding

to the semi-stable limit cycle F. Curves corresponding to heteroclinic connections between the saddles are denoted with the letter H and are labeled by the saddle from which they leave. Thus the curve corresponding to a heteroclinic connection from L to M is denoted H_L. We obtain the following bifurcation diagrams.

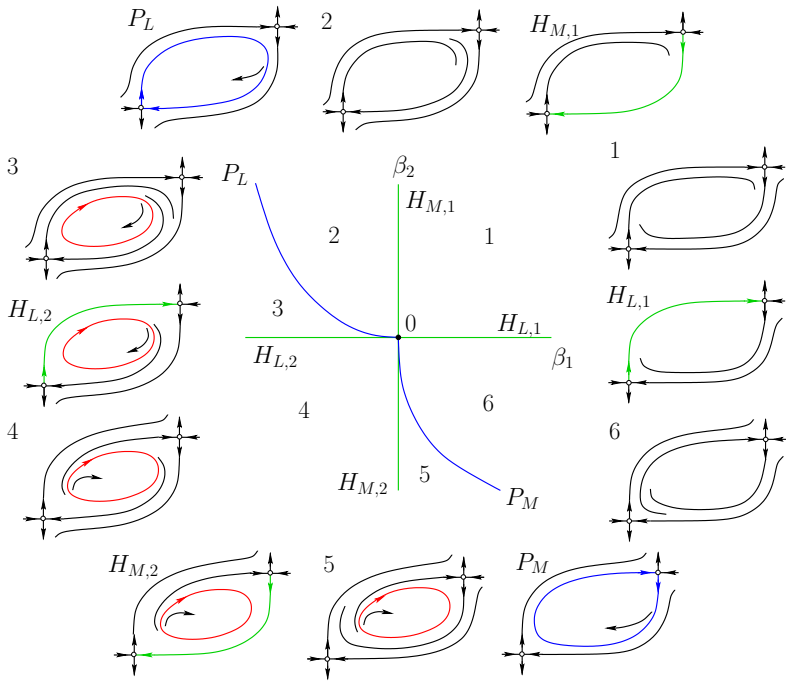

Figure 5.7: $\lambda < 1$ and $\mu < 1$

Choosing parameter values on the curve P_L and varying the parameters through the bifurcation diagram (Figure 5.7) counterclockwise, we observe the following evolution of the phase portrait.

We begin with a small homoclinic connection at the saddle L. This homoclinic connection is broken outwards and an unstable limit cycle is generated which is in accordance with the fact that $\lambda < 1$. After some time, a heteroclinic connection from L to M is formed and destroyed, and thereafter the same happens for a heteroclinic connection from M to L. Eventually, the unstable limit cycle disappears to form a small homoclinic connection at M which is then broken inwards. This generates no limit cycles in accordance with the fact that $\lambda < 1$. Under further variation of

the parameters, heteroclinic connections from L to M and back are formed and destroyed before the original homoclinic connection at L is again formed.

In short, one might describe these dynamics as the interplay between two homoclinic bifurcations.

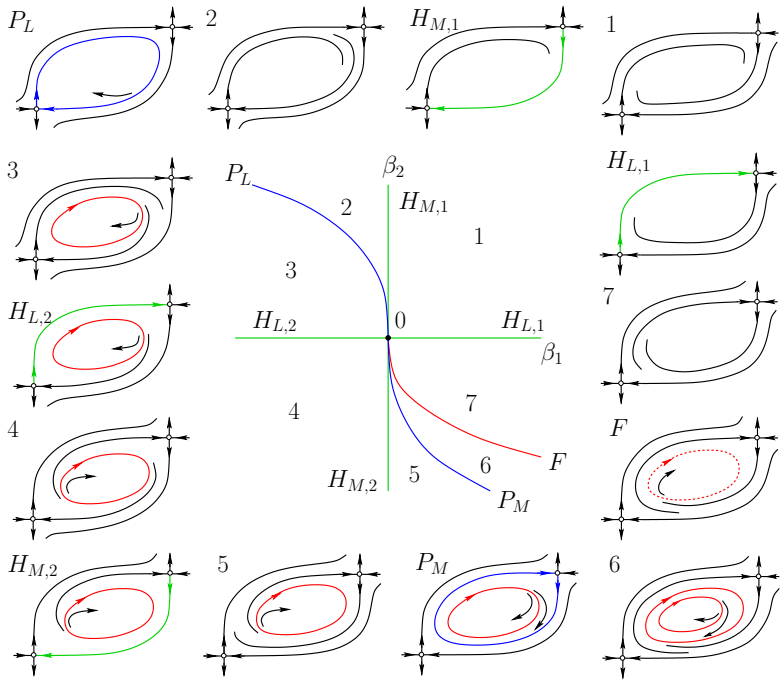

Figure 5.8: $\lambda < 1$ and $\mu > 1$

In the second subcase we perform the same analysis. Starting out with parameter values on P_L and varying them counterclockwise through the bifurcation diagram (Figure 5.8) we start with a small homoclinic connection at L which is destroyed forming an unstable limit cycle. This behaviour is not different from the first subcase, which was to be expected as it still holds that $\lambda < 1$.

The evolution of the phase portrait does not differ from the first subcase until a small homoclinic connection at M is formed. In this process, the unstable limit cycle does not disappear but is contained within the homoclinic connection. This is in accordance with the fact that $\mu > 1$. Furthermore, when this connection is broken inwards another, now stable, limit cycle is generated en-

closing the original unstable limit cycle. Eventually, these limit cycles collide forming a single limit cycle which is stable from the outside but unstable from the inside. This semi-stable limit cycle is immediately destroyed and further variation of the parameters only forms heteroclinic connections from L to M and back before the original homoclinic connection at L is again formed.

In short, one might describe these dynamics as the interplay between two homoclinic bifurcations resulting in a fold of cycles bifurcation.

6 The non-monodromic case

We now proceed to the non-monodromic case. The treatment will be analogous to that of the monodromic case. Thus, we begin by studying homoclinic connections, then move to limit cycles and their bifurcations and then heteroclinic connections. Once more, this will be enough to sketch the bifurcation diagram in both subcases.

Many of the results on the non-monodromic case will be similar to previous results. Once more, we will be able to find two curves, P_L and P_M, corresponding to homoclinic connections at L and M which we use to divide the parameter-plane into two sectors.

In the first subcase ($\lambda < 1$ and $\mu < 1$) we find that in one of the sectors no limit cycles are present. If we continuously vary our parameters from this sector into the other sector we cross its border either through P_L or P_M. Breaking either on of the associated homoclinic connections generates an unstable limit cycle at a homoclinic bifurcation. If we vary the parameters further, a homoclinic connection at the opposing saddle is generated and then destroyed, also destroying the unstable limit cycle.

In the second subcase ($\lambda < 1$ and $\mu > 1$) the first sector still does not contain any limit cycles. We may once more break the homoclinic connection at L to generate an unstable limit cycle. Varying the parameters further, a homoclinic connection appears at M, now with $\mu > 1$. As a result of this difference, breaking of the homoclinic connection does not destroy the unstable limit cycle, but generates an additional stable limit cycle enclosing it. Eventually, these limit cycles collide, momentarily forming a semi-stable limit cycle at a fold of cycles bifurcation.

We recognize that all these results are similar to the monodromic case. However, the non-monodromic case also presents

a new phenomenon. In the non-monodromic case there may be non-trivial heteroclinic connections, that is, heteroclinic connections which appear when both splitting parameters are non-zero. These connections must wind around L at least once before reaching L or M.

Actually, in both subcases, there exist two infinite series of curves corresponding to heteroclinic connections between the saddles with each connection making an increasing number of turns. Thus, we encounter the phenomenon of flashing heteroclinic connections, both at the bifurcation of a semi-stable limit cycle as well as a homoclinic connection. In the parameter plane, the infinite series of curves corresponding to these non-trivial heteroclinic connections accumulate, in the first subcase at P_L and P_M, corresponding to the homoclinic connections, and in the second subcase at P_L and F, corresponding to the semi-stable limit cycle.

The results and techniques in this section are due to [7].

6.1 Homoclinic connections

As in the monodromic case, the emergence of a homoclinic connection at L coincides with a solution of the equation

$$(R \circ \Delta_M \circ Q)(0) = \beta_1 - \theta_2 \beta_2^{\mu} = 0 \tag{6.1}$$

which we rewrite as

$$\beta_2 = \left(\frac{\beta_1}{\theta_2}\right)^{\frac{1}{\mu}}$$

expressing β_2 in terms of β_1.

For saddles at M we again solve

$$(Q \circ \Delta_L \circ R)(0) = \beta_2 - \theta_1 \beta_1^{\lambda} = 0 \tag{6.2}$$

which becomes

$$\beta_2 = \theta_1 \beta_1^{\lambda}.$$

Once more, we have obtained the curves P_L and P_M in the parameter-plane corresponding to homoclinic connections. We sketch these curves in both relevant cases in Figure 6.1.

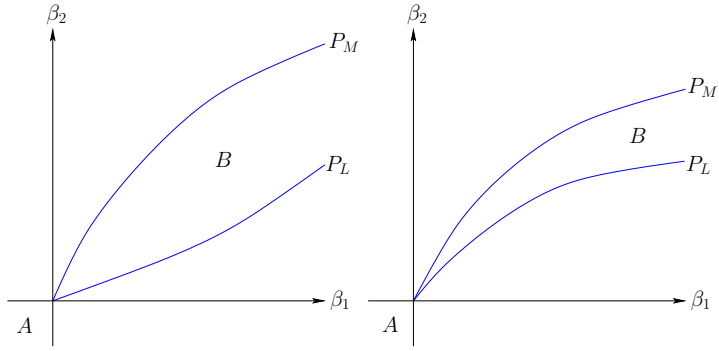

(a) $\lambda < 1$ and $\mu > 1$ (b) $\lambda < 1$ and $\mu < 1$

Figure 6.1: The emergence of homoclinic connections in the parameter-plane

Both sets of curves in the parameter-planes divide the planes into two sectors. Again, we denote these sectors A and B.

6.2 Limit cycles

The geometry of the non-monodromic contour does not allow the generation of limit cycles near the contour when one of the splitting parameters is negative. This can for example be seen from Figure (6.2).

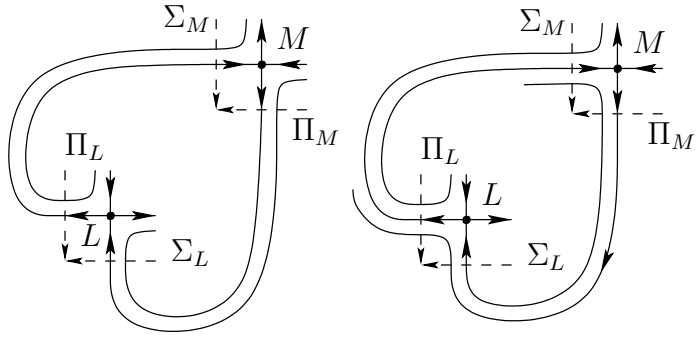

(a) Both parameters negative (b) Parameters of opposite sign

Figure 6.2: Negative parameter values prohibit the generation of homoclinic connections

Thus, we may restrict our attention to non-negative values of the parameters when looking for the emergence of limit cycle.

To study the appearance of limit cycles we again look for fixed points of the Poincaré map which now becomes (4.2). Thus, we look for solutions ξ_L of

$$\beta_1 - \theta_2(\beta_2 - \theta_1\xi_L^\lambda)^\mu = \xi_L$$

which we may rewrite to the equation

$$\beta_2 - \theta_1\xi_L^\lambda = \left(\frac{\beta_1 - \xi_L}{\theta_2}\right)^{\frac{1}{\mu}}. \tag{6.3}$$

Considering the left- and right-hand sides as separate functions, we define f and g by

$$f(\xi_L) = \beta_2 - \theta_1\xi_L^\lambda \quad \text{and} \quad g(\xi_L) = \left(\frac{\beta_1 - \xi_L}{\theta_2}\right)^{\frac{1}{\mu}}$$

which allow us to rewrite (6.3) as $f(\xi_L) = g(\xi_L)$.

To look for solutions of this equation we study the derivatives of f and g which we find to be

$$f'(\xi_L) = -\lambda\theta_1\xi_L^{\lambda-1} \quad \text{and} \quad g'(\xi_L) = -\frac{1}{\mu\theta_2}\left(\frac{\beta_1 - \xi_L}{\theta_2}\right)^{\frac{1}{\mu}-1}.$$

Just as in the monodromic case the maps f and g have a geometric interpretation as maps from Σ_L to Σ_M and again a solution $f(0) = g(0)$ coincides with a homoclinic connection at L while a solution $\xi_L \neq 0$ satisfying $f(\xi_L) = g(\xi_L) = 0$ coincides with a homoclinic connection at M.

Furthermore, we have expressions for

$$f(0) = \beta_2 \quad \text{and} \quad g(0) = \left(\frac{\beta_1}{\theta_2}\right)^{\frac{1}{\mu}}$$

and we can find solutions to $f(\xi_L^f) = 0$ and $g(\xi_L^g) = 0$, namely

$$\xi_L^f = \left(\frac{\beta_2}{\theta_1}\right)^{\frac{1}{\lambda}} \quad \text{and} \quad \xi_L^g = \beta_1.$$

This allows us to relate the parameters in sectors A and B to configurations of f and g.

6.2.1 The first subcase

In this case we have that $\lambda < 1$ and $\mu < 1$. The maps f and g have the limiting properties

$$\lim_{\xi_L \downarrow 0} f(\xi_L) = \beta_2 \quad \text{and} \quad \lim_{\xi_L \downarrow 0} f'(\xi_L) = -\infty$$

while

$$\lim_{\xi_L \uparrow \beta_1} g(\xi_L) = 0 \quad \text{and} \quad \lim_{\xi_L \uparrow \beta_1} g'(\xi_L) = 0$$

which tells us that both f and g are convex downwards.

Similar to the monodromic case, f and g can not have equal derivative for arbitrarily small values of the parameters. In this, $f'(\xi_L) = g'(\xi_L)$ implies

$$-\lambda\theta_1\xi_L^{\lambda-1} = -\frac{1}{\mu\theta_2}\left(\frac{\beta_1 - \xi_L}{\theta_2}\right)^{\frac{1}{\mu}-1}.$$

We may now rewrite this into the expression

$$\beta_1 = \xi_L + \theta_2(\lambda\mu\theta_1\theta_2)^{\frac{\mu}{1-\mu}}\xi_L^{\frac{\mu(\lambda-1)}{1-\mu}}.$$

Noting again that $\frac{\mu(\lambda-1)}{1-\mu} < 0$ by our assumption on λ and μ we see that $\lim_{\xi_L \downarrow 0} \beta_1(\xi_L) = \infty$. Thus, letting ξ_L as well as the parameters go to zero, f and g can not have the same derivative at ξ_L and we may also find at most one intersection for small values of ξ_L and the parameters.

Suppose that we choose a pair of parameters from sector A. This pair lies either above or below P_L and P_M. Suppose the pair lies below them, then

$$\beta_2 < \left(\frac{\beta_1}{\theta_2}\right)^{\frac{1}{\mu}} \quad \text{so} \quad f(0) < g(0)$$

and

$$\beta_2 < \theta_1\beta_1^{\lambda} \quad \text{so} \quad \xi_L^f < \xi_L^g.$$

If the pair lies above P_L and P_M the inequalities are reversed so $f(0) > g(0)$ and $\xi_L^f > \xi_L^g$. In either case, there will be no intersections for small values of the parameters, which we can see from Figure 6.3a and 6.3b. The graphs might suggest that tangency is possible but we have just noted that for small enough values of the parameters this is impossible. We conclude that no limit cycles are present for parameters from sector A.

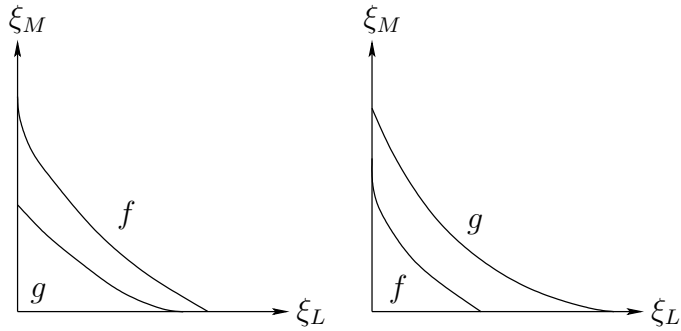

(a) No intersections (b) No intersections

Figure 6.3: The graphs of f and g for parameters in sector A

Parameters in sector B are found above P_L but below P_M. Thus, we find that $f(0) > g(0)$ while $\xi_L^f < \xi_L^g$. In this case, there is an intersection for small values of the parameters as can be seen in Figure 6.4a. We conclude that there is one limit cycle for parameter values in sector B.

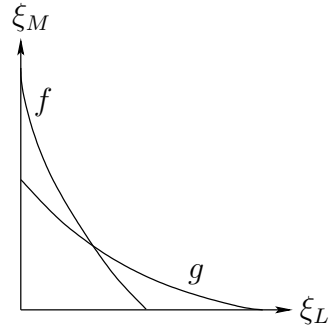

(a) One intersection

Figure 6.4: The graph of f and g for parameters in sector B

6.2.2 The second subcase

Moving to the second subcase ($\lambda < 1$ and $\mu > 1$), the maps f and g have the limiting properties

$$\lim_{\xi_L \downarrow 0} f(\xi_L) = \beta_2 \quad \text{and} \quad \lim_{\xi_L \downarrow 0} f'(\xi_L) = -\infty$$

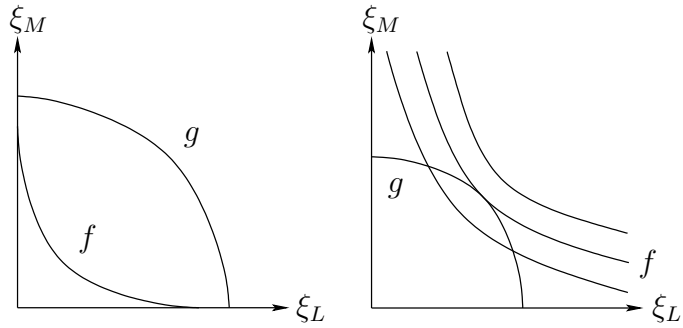

(a) No intersections

(b) Zero, one or two intersections

Figure 6.5: The graphs of f and g for parameters in sector A

while

$$\lim_{\xi_L \uparrow \beta_1} g(\xi_L) = 0 \quad \text{and} \quad \lim_{\xi_L \uparrow \beta_1} g'(\xi_L) = \infty$$

which tells us that both f is convex downwards and g is convex upwards.

If we choose parameters from sector A, we find as above that if we choose parameters below the curves P_L and P_M so $f(0) < g(0)$ and $\xi_L^f < \xi_L^g$ there will be no cycles generated, see Figure 6.5a. Alternatively, we choose parameters above P_L and P_M yielding $f(0) > g(0)$ and $\xi_L^f > \xi_L^g$. In this case we find that either there are two intersections, one intersection when f and g are tangent or no intersections for increasing values of β_2 see Figure 6.5b. As in the monodromic case, we see that this corresponds with a fold of cycles bifurcation.

Lastly, we consider parameter values from sector B implying $f(0) > g(0)$ and $\xi_L^f < \xi_L^g$. In this case, we see that there is one intersection, as pictured in Figure 6.6a.

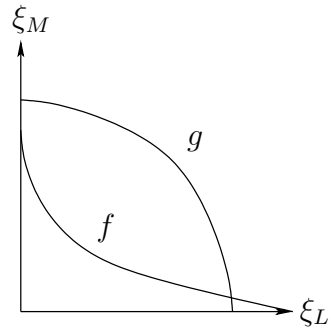

(a) One intersection

Figure 6.6: The graph of f and g for parameters in sector B

6.2.3 Semi-stable cycle

As in the monodromic case, we are interested in the parameters values for which a semi-stable cycle exist. Specifically, we would like to express β_2 in terms of β_1 for these parameter-values. The same conditions hold as in the monodromic case, except that we are now in the non-monodromic case which in terms of the parameters can be reached by the transformation $(\theta_1, \theta_2) \mapsto (-\theta_1, -\theta_2)$. Thus we can derive an expression for β_2 in terms of β_1 by applying this transformation to (5.4), yielding

$$\beta_2 = \theta_2 \beta_1^{\lambda} - (1-\mu^{\mu})(\lambda\mu\theta_1\theta_2)^{\frac{1}{1-\mu}} \beta_1^{\frac{\lambda-1}{1-\mu}}. \tag{6.4}$$

6.3 Heteroclinic connections

As in the monodromic case, a heteroclinic connection exists whenever one of the parameters is zero. However, as opposed to the monodromic case, the non-monodromic case may exhibit heteroclinic connections when both parameters are nonzero. For this to happen, a connection must wind around the saddle L at least once before making a connection. As we shall see, there exist infinite series of curves in the parameter plane corresponding to heteroclinic connections making an increasing number of windings around the L, a phenomenon introduced in Section 3.4 as flashing heteroclinic connections.

In both subcases, vector fields for parameter values in sector B contain a limit cycle which separates the saddles, making a

heteroclinic connection impossible. In the first subcase, this obstruction to heteroclinic connections disappears when a homoclinic connection is formed and immediately destroyed at either one of the saddles. Indeed, we are in the situation of Theorem 3.4 which shows that in sector A, two infinite series of curves corresponding to flashing heteroclinic connections exist which accumulate at P_L and P_M.

In the second subcase the situation at P_L is the same as in the first subcase. However, at the destruction of P_M, a second, now stable, limit cycle is born, further prohibiting the formation of heteroclinic connections. Eventually, after the two limit cycles have collided to form a critical semi-stable cycle which then disappears, heteroclinic connections are again possible. In fact, we recognize that we are in the situation of the original flashing heteroclinic connections of [10] so Theorem 3.3 shows that in this case there exists a second infinite series of curves in A corresponding to heteroclinic connections which accumulates at F.

6.4 Sketching the bifurcation diagram

Summarising the results of both non-monodromic subcases we sketch the bifurcation diagrams of both cases. We use the same notation for curves corresponding to homoclinic connections and semi-stable limit cycles. The curves corresponding to heteroclinic connections are indicated along with the number of turns around the saddle L, indicated as a bracketed subscript. We only supply phase portraits for heteroclinic connections making at most one turn. The accumulating curves corresponding to the connections making more turns are drawn dashed. We obtain the following bifurcation diagrams.

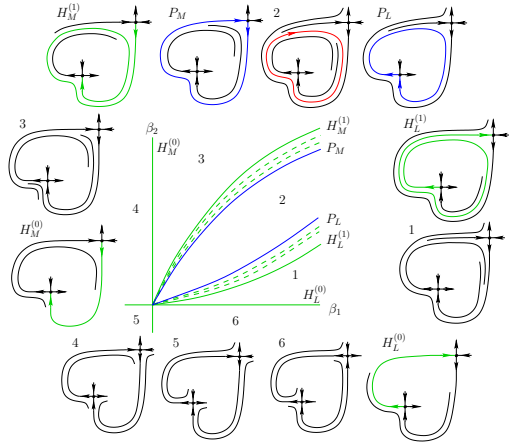

Figure 6.7: $\lambda < 1$ and $\mu < 1$

Choosing parameter values on the curve $H_L^{(0)}$ and varying the parameters through the bifurcation diagram (Figure 6.7) counterclockwise, we observe the following evolution of the phase portrait.

At the outset, there is a heteroclinic connection from L to M which is destroyed. After variation of the parameters, a second heteroclinic connection is formed which winds around the saddle L once before reaching M. Varying the parameters further results in an infinite series of heteroclinic connections from L to M making an increasing number of turns around L before eventually a big homoclinic connection at L is formed. This big homoclinic connection is broken inwards, generating an unstable limit cycle in accordance with the fact that $\lambda < 1$. This limit cycle disappears when a small homoclinic connection at M is formed, in accordance with $\mu < 1$. Breaking this homoclinic connection results again in an infinite number of heteroclinic connections, now from M to L and making a decreasing number of turns. After further variation of the parameters the original heteroclinic connection from L to M is formed again.

In short, the dynamics of this situation may be described as the interplay between to homoclinic bifurcations in the presence of two series of flashing heteroclinic connections.

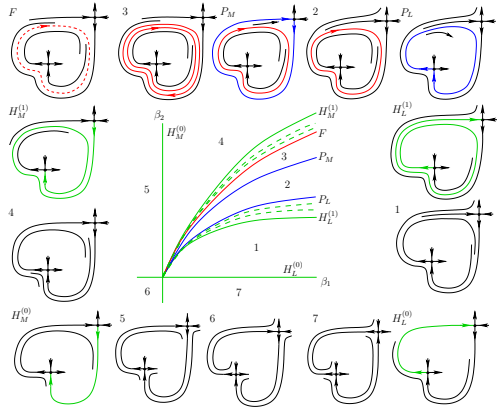

Figure 6.8: $\lambda < 1$ and $\mu > 1$

Performing the same analysis in the second subcase (see Figure 6.8) yields the same result up to the appearance of a small homoclinic connection at M. In accordance with the fact that $\mu > 1$, the existing unstable limit cycle is not destroyed in this process. As in the monodromic case, the destruction of this small homoclinic loop generates a stable limit cycle enclosing the stable one. Eventually these two cycles collide, momentarily forming a limit cycle which is stable from the outside but unstable from the inside. In this case, an infinite series of heteroclinic connections from M to L accumulates at this semi-stable limit cycle. Thus, when this limit cycle is destroyed we again encounter an infinite series of heteroclinic connections from M to L making a decreasing number of turns around L. The further behaviour is the same as in the first subcase.

These dynamics may be described as the interplay between two homoclinic bifurcations yielding a fold of cycles bifurcation in the presence of two series of flashing heteroclinic connections.

Part IV
Two polynomial examples

In this part of the thesis we will present two systems of polynomial ordinary differential equations which will illustrate some of the theoretical results obtained in the previous part. These explicit examples allow for numerical computation of the various phase objects and bifurcation diagrams using MatCont [5, 6, 3], which are then to be compared to their theoretically predicted counterparts.

Our strategy to find explicit monodromic examples, originally due to [12] and introduced in Section 3.1.1, will be to look for an algebraic variety which has the shape of the monodromic contour and then to look for vector fields which are tangent to this variety. For a non-monodromic example a different construction is necessary. It is based on the idea of perturbing a reversible system containing a big homoclinic connection.

7 A monodromic example

7.1 Derivation of the example

To construct a vector field containing a monodromic heteroclinic contour, we will again look for an algebraic variety which has a shape similar to such a contour. For this example we choose the union of a parabola with the x-axis. Specifically, we choose the parabola described by $y = x(1-x)$, see Figure 7.1.

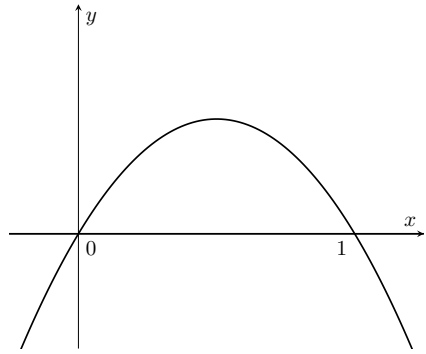

Figure 7.1: The union of the parabola $y = x(1-x)$ with the x-axis.

This algebraic variety can be realised as the zero-set of the function

$$G(x,y) = y(y - x(1-x)) \tag{7.1}$$

and we write $\Gamma = G^{-1}(0)$.

Our next step is to look for two polynomial equations $P(x,y)$ and $Q(x,y)$ such that the vector field defined by

$$\begin{cases} \dot{x} = P(x,y) \\ \dot{y} = Q(x,y) \end{cases} \tag{7.2}$$

is tangent Γ. For this to happen it must hold that

$$\langle \nabla G(x,y), \begin{pmatrix} P(x,y) \\ Q(x,y) \end{pmatrix} \rangle = 0 \tag{7.3}$$

for all $(x,y) \in \Gamma$. The equation (7.3) will yield conditions from which we can derive preliminary expressions for $P(x,y)$ and $Q(x,y)$. As we will soon see, it will suffice to use polynomials of second degree. Thus, we set

$$\begin{cases} P(x,y) = a_{00} + a_{10}x + a_{01}y + a_{20}x^2 + a_{11}xy + a_{02}y^2, \\ Q(x,y) = b_{00} + b_{10}x + b_{01}y + b_{20}x^2 + b_{11}xy + b_{02}y^2. \end{cases} \tag{7.4}$$

Then, (7.3) yields the system of equations

$$\begin{cases} 2a_{00}x - 3a_{00}x^2 + 2a_{10}x^2 - 3a_{10}x^3 + 2a_{20}x^3 - 3a_{20}x^4 \\ \quad - 2b_{00}y + 2a_{01}xy - 2b_{10}xy - 3a_{01}x^2y + 2a_{11}x^2y \\ \quad - 2b_{20}x^2y - 3a_{11}x^3y - 2b_{01}y^2 + 2a_{02}xy^2 - 2b_{11}xy^2 \\ \quad - 3a_{02}x^2y^2 - 2b_{02}y^3 = 0 \\ y^2 - xy + x^2y = 0 \end{cases} \tag{7.5}$$

To study this polynomial system we use the software package Mathematica to calculate its Gröbner basis using the elimination order as monomial order. This yields a total of five basis polynomials including $G(x,y)$ itself. To look for solutions of (7.5) we choose the shortest basis polynomial and look for choices of the coefficients which render this polynomial identically zero. This yields

the system of linear equations

$$\begin{cases} 2b_{00} - a_{00} = 0 \\ b_{01} - 2b_{20} - a_{20} - 2a_{10} - a_{01} = 0 \\ b_{02} - 2a_{11} - a_{02} = 0 \\ -b_{00} = 0 \\ 2a_{00} + a_{10} + a_{20} + 2b_{10} + 2b_{20} = 0 \\ 2a_{01} + a_{11} - 2a_{20} + b_{11} + 2a_{02} = 0 \\ b_{00} - b_{10} = 0 \\ b_{10} - b_{20} = 0 \\ b_{20} = 0 \end{cases} \tag{7.6}$$

which is solved whenever we set $a_{20} = -a_{10}$, $b_{01} = a_{01} + a_{10}$, $b_{11} = -2a_{01} - 2a_{10} - a_{11}$, $b_{02} = 2a_{11}$ and all remaining coefficients to zero. We see that this leaves us with three free parameters remaining. Renaming $a_{10} = a$, $a_{01} = b$ and $a_{11} = c$ and substituting the solution of (7.6) into $p(x, y)$ and $Q(x, y)$ we get the preliminary expressions

$$\begin{cases} P(x, y) = ax + by + cxy - ax^2, \\ Q(x, y) = (a + b)y - (2a + 2b + c)xy + 2cy^2. \end{cases} \tag{7.7}$$

Using (7.2) we now obtain a vector field

$$\begin{cases} \dot{x} = ax + by + cxy - ax^2, \\ \dot{y} = (a + b)y - (2a + 2b + c)xy + 2cy^2. \end{cases} \tag{7.8}$$

for any choice of a, b and c.

As expected, this vector field always has equilibria $L = (0, 0)$ and $M = (1, 0)$. However, the types of these equilibria depend on the values of a, b and c. To see this, we calculate the eigenvalues of the linearised systems at these points. The Jacobian matrix of this vector field is given by

$$J(x, y) = \begin{pmatrix} a - 2ax + cy & b + cx \\ -(2a + 2b + c)y & a + b - (2a + 2b + c)x + 4cy \end{pmatrix}. \tag{7.9}$$

From this we calculate the eigenvalues at $(0, 0)$ to be a and $a + b$ and the eigenvalues at $(1, 0)$ to be $-a$ and $-a - b - c$.

As a first example, we set $a = 1$, $b = -3$ and $c = 3/2$. We find that $\lambda_u = 1$ and $\lambda_s = -2$ so $\lambda = -\lambda_s/\lambda_u = 2 > 1$, while $\mu_u = 1/2$

and $\mu_s = -1$ so $\mu = -\mu_s/\mu_u = 2 > 1$. Obviously, $\lambda\mu > 1$ implying that the heteroclinic contour is stable from inside. We recognize that these saddle indices correspond to the first subcase treated in Section 5, *after the time reversal*. A phase portrait of this system is given in Figure 7.2.

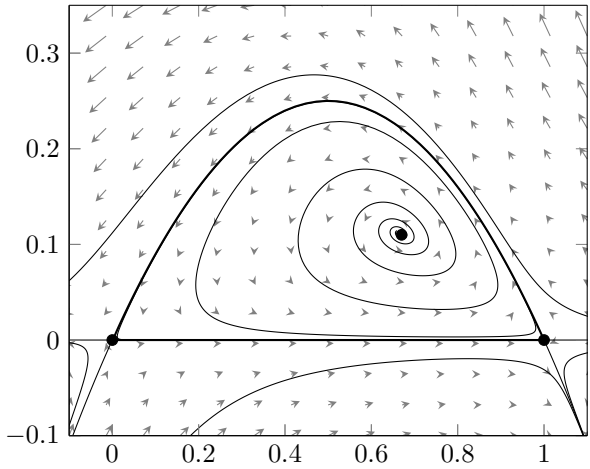

Figure 7.2: Phase portrait of (7.8) for $a = 1$, $b = -3$ and $c = 3/2$

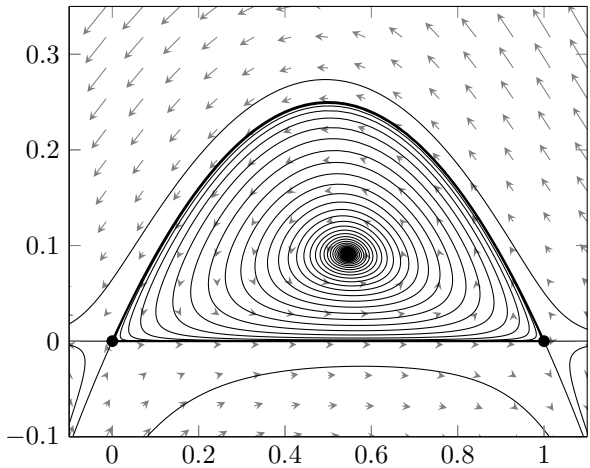

Figure 7.3: Phase portrait of (7.8) for $a = 1$, $b = -3$ and $c = 1/2$

As a second example, we set $a = 1$, $b = -3$ and $c = 1/2$. Then it remains that $\lambda = 2 > 1$ but now $\mu_u = 3/2$ and $\mu_s = -1$ so $\mu = -\mu_s/\mu_u = 2/3 < 1$ and $\lambda\mu = 4/3 > 1$. We recognize that we are in the situation of the second subcase treated in Section 5. A phase portrait of this system is displayed in Figure 7.3.

In order to perform bifurcation analysis we still need to add two parameter-dependent perturbing terms to (7.8) which break the heteroclinic connections separately. As these connections can be described by the equations $y = x(1 - x)$ and $y = 0$ this can be achieved by choosing parameters α and ε and adding the perturbing terms $\alpha(y - x(1 - x))$ and εy to (7.8). It is clear that the first perturbation does not affect the parabola while the second perturbation does not affect the straight line.

We add one perturbing term to $\dot{x}$ and one to $\dot{y}$. This yields

$$\begin{cases} \dot{x} = ax + by + cxy - ax^2 + \varepsilon y, \\ \dot{y} = (a + b)y - (2a + 2b + c)xy + 2cy^2 + \alpha(y - x(1 - x)). \end{cases} \tag{7.10}$$

7.2 Numerical analysis of the example

Using the software package Matcont [5, 6, 3] we perform numerical analysis of the system (7.10) in both subcases. More specifically, we will be able to locate and continue homoclinic connections and cycles which will allow us to approximate the bifurcation diagrams of both subcases.

Section 5 resulted in a general sketch of these diagrams (see Figure 5.2). The numerical study of these polynomial systems will allow us to compare this general diagram based on the behaviour of model maps to an actual example of such a diagram.

This analysis in the first case yields the bifurcation diagram displayed in Figure 7.4.

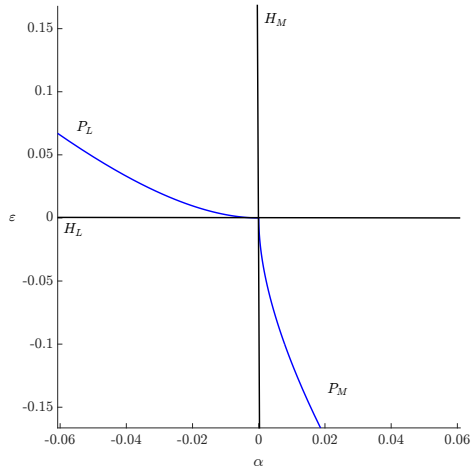

Figure 7.4: The parameter plane diagram in the first subcase ($a = 1$, $b = -3$ and $c = 3/2$)

This analysis in the second case yields the bifurcation diagram displayed in Figure 7.5.

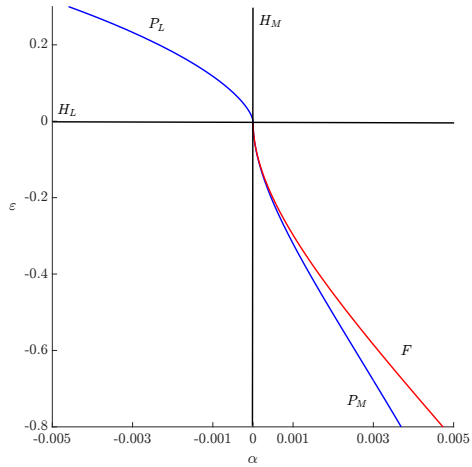

Figure 7.5: The parameter plane diagram in the second subcase ($a = 1$, $b = -3$ and $c = 1/2$)

To complete our analysis of these systems we compute representative phase portraits for parameter values in all components

of the bifurcation diagrams. The contents of these phase portraits were already predicted in the previous part. They are displayed in Figures 7.6 and 7.7.

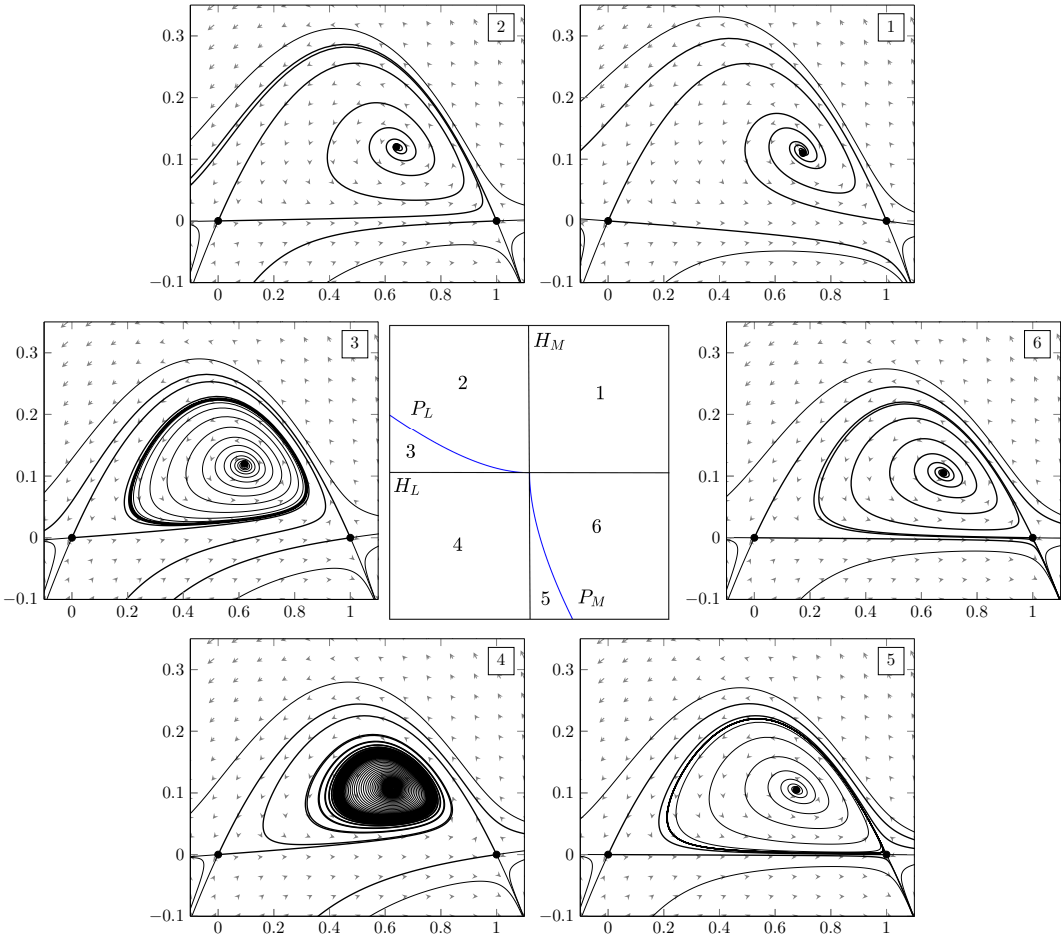

Figure 7.6: The full bifurcation diagram for the first subcase

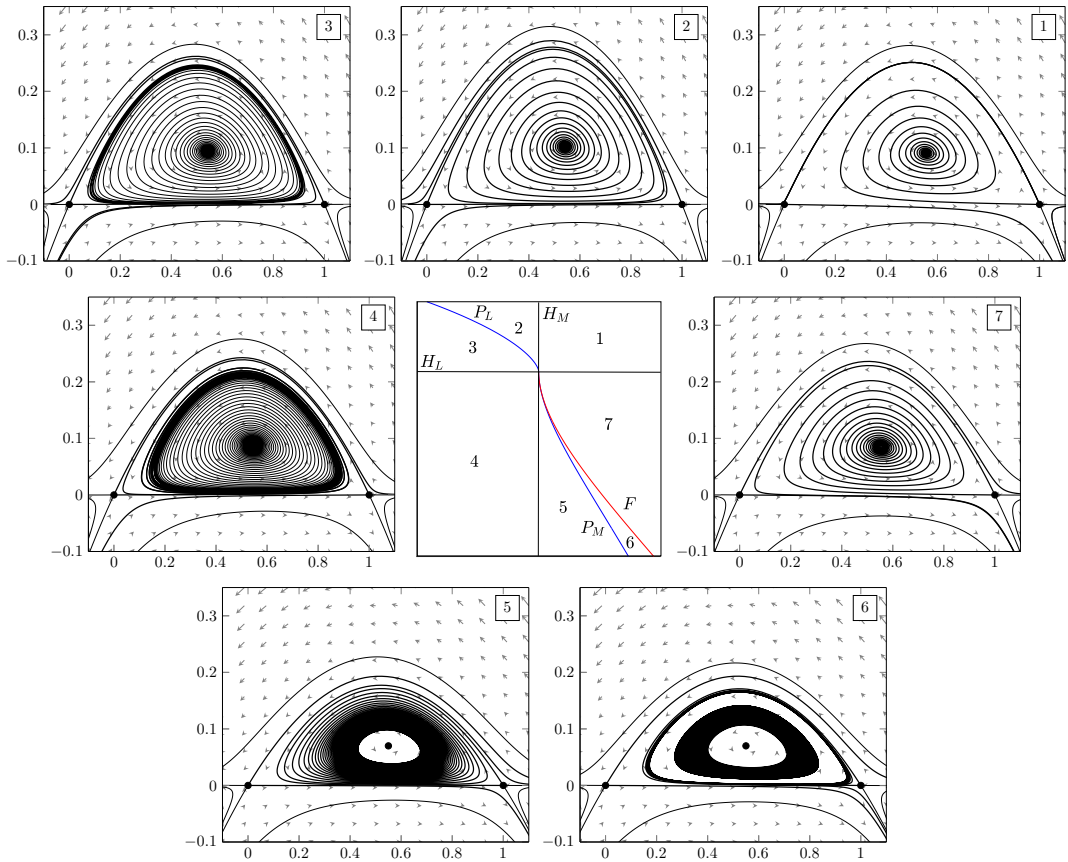

Figure 7.7: The full bifurcation diagram for the second subcase

8 A non-monodromic example

8.1 Finding an example

The starting point is the following reversible system[2]

$$\begin{cases} \dot{x} &= y, \\ \dot{y} &= x + xy - x^3, \end{cases} \tag{8.1}$$

that has a saddle $(0,0)$, a stable focus $(-1,0)$, and an unstable focus $(1,0)$. The saddle at the origin has a 'big' homoclinic orbit, while

[2]The system is invariant under the involution $(t,x,y) \mapsto (-t,-x,y)$.

both foci are located inside the domain bounded by the homoclinic loop as seen in Figure 8.1.

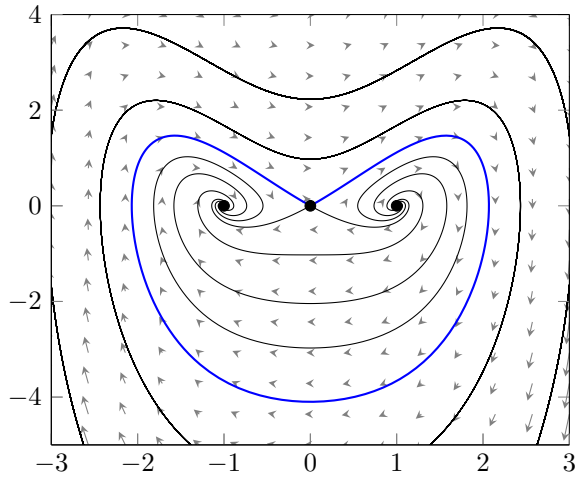

Figure 8.1: System (8.1) containing a big homoclinic loop

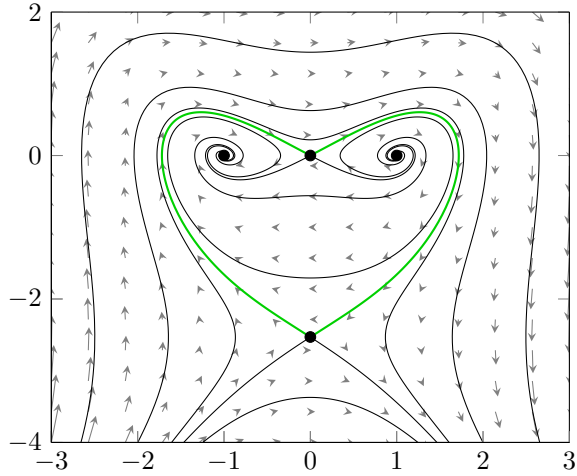

Figure 8.2: The symmetric non-monodromic heteroclinic contour in the reversible system (8.2) with $\gamma = \gamma_0$.

The one-parameter modification of (8.1) that preserves the reversibility,

$$\begin{cases} \dot{x} &= y(y+\gamma), \\ \dot{y} &= x + xy - x^3, \end{cases} \tag{8.2}$$

has an additional saddle at $(0, -\gamma)$. This saddle is connected to the saddle at $(0, 0)$ by two heteroclinic orbits when $\gamma_0 = 2.5315\ldots$ (see Figure 8.2). Of course, both saddles of (8.2) are neutral.

To break reversibility, introduce the following two-parameter deformation of (8.2):

$$\begin{cases} \dot{x} &= \varepsilon x + y(y+\gamma), \\ \dot{y} &= \alpha y + x + xy - x^3. \end{cases} \tag{8.3}$$

This system still has a saddle at $(0, 0)$, while the second saddle moves off the y-axis. In order to obtain a generic non-monodromic heteroclinic contour, all three parameters of (8.3) have to vary. Since the existence of such heteroclinic contour is a codim 2 phenomenon, we expect a curve in the $(\alpha, \varepsilon, \gamma)$-space passing through $(0, 0, \gamma_0)$, along which the contour persists.

8.2 Numerical analysis of the example

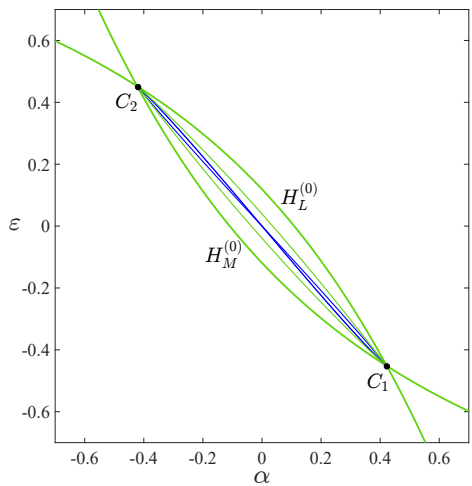

Figure 8.3: Partial bifurcation diagram of (8.3) with $\gamma = 2.7$: heteroclinic bifurcation curves (green), primary homoclinic curves (blue).

The main curves of the bifurcation diagram of (8.3) in the (α, ε)-plane at $\gamma = 2.7$ is shown in Figure 8.3. Since the transformation $(t, x, \alpha, \varepsilon) \mapsto (-t, -x, -\alpha, -\varepsilon)$ preserves the system (8.3), its bifurcation diagram is invariant under the inversion $(\alpha, \varepsilon) \mapsto (-\alpha, -\varepsilon)$.

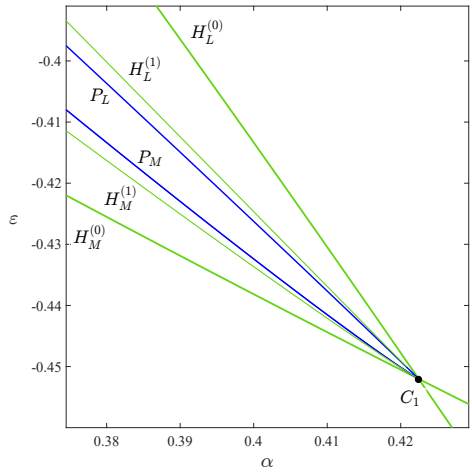

Figure 8.4: Partial bifurcation diagram of (8.3) near the lower codim 2 point C_1: primary and secondary heteroclinic bifurcation curves $H_{L,M}^{(k)}$ (green), primary homoclinic curves $P_{L,M}$(blue).

There are two non-monodromic heteroclinic contours at the intersection points $C_{1,2}$ of the heteroclinic curves $H_{L,M}^{(0)}$. These points are the end-points of two primary homoclinic curves $P_{L,M}$, which also intersect at $(\alpha, \varepsilon) = (0, 0)$, where two independent homoclinic orbits to both saddles exist. Since the system is reversible at $\alpha = \varepsilon = 0$, both homoclinic orbits are symmetric. All orbits in the annulus bounded by these two homoclinic orbits are periodic.

The lower heteroclinic contour point

$$C_1 = (\alpha, \varepsilon) = (0.422432\ldots, -0.452007\ldots).$$

The corresponding phase portrait is shown in Figure 8.5. The saddles at these parameter values are

$$L = (0, 0) \quad \text{and} \quad M = (-0.57039\ldots, -2.6009\ldots),$$

with eigenvalues

$$\lambda_s = -1.7151\ldots, \quad \lambda_u = 1.6856\ldots$$

and

$$\mu_s = -2.8436\ldots, \quad \mu_u = 2.2436\ldots,$$

respectively. The corresponding indices are

$$\lambda = -\frac{\lambda_s}{\lambda_u} = 1.0175\ldots > 1 \quad \text{and} \quad \mu = -\frac{\mu_s}{\mu_u} = 1.2674\ldots > 1.$$

Notice that both saddles in this heteroclinic contour are dissipative.

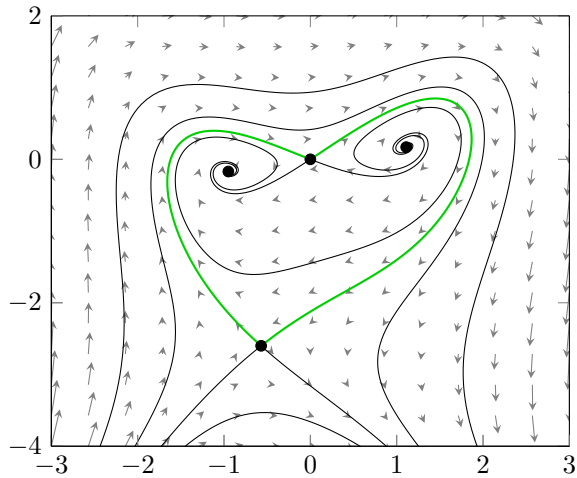

Figure 8.5: Non-monodromic heteroclinic contour in system (8.2) with $\gamma = 2.7$ at codim 2 point C_1.

The upper heteroclinic contour point

$$C_2 = (\alpha, \varepsilon) = (-0.422432\ldots, 0.452007\ldots).$$

The corresponding phase portrait is shown in Figure 8.6. The saddles at these parameter values are

$$L = (0, 0) \quad \text{and} \quad M = (0.570399\ldots, -2.6009\ldots),$$

with the eigenvalues

$$\lambda_s = -1.6856\ldots, \quad \lambda_u = 1.7151\ldots$$

and

$$\mu_s = -2.2436\ldots, \quad \mu_u = 2.8436\ldots,$$

respectively. The corresponding indices are

$$\lambda = -\frac{\lambda_s}{\lambda_u} = 0.982\ldots < 1 \quad \text{and} \quad \mu = -\frac{\mu_s}{\mu_u} = 0.789\ldots < 1.$$

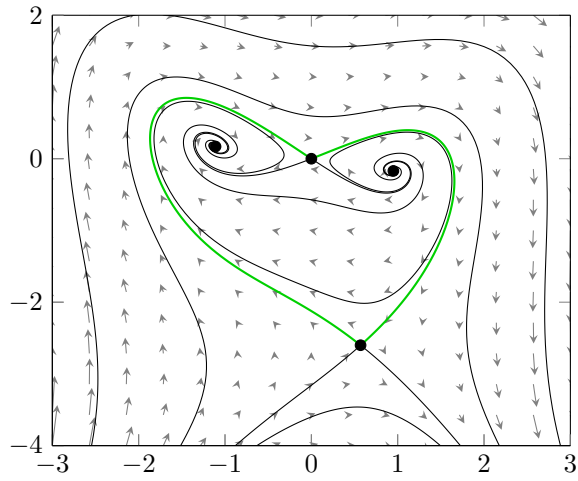

Figure 8.6: Non-monodromic heteroclinic contour in system (8.3) with $\gamma = 2.7$ at codim 2 point C_2.

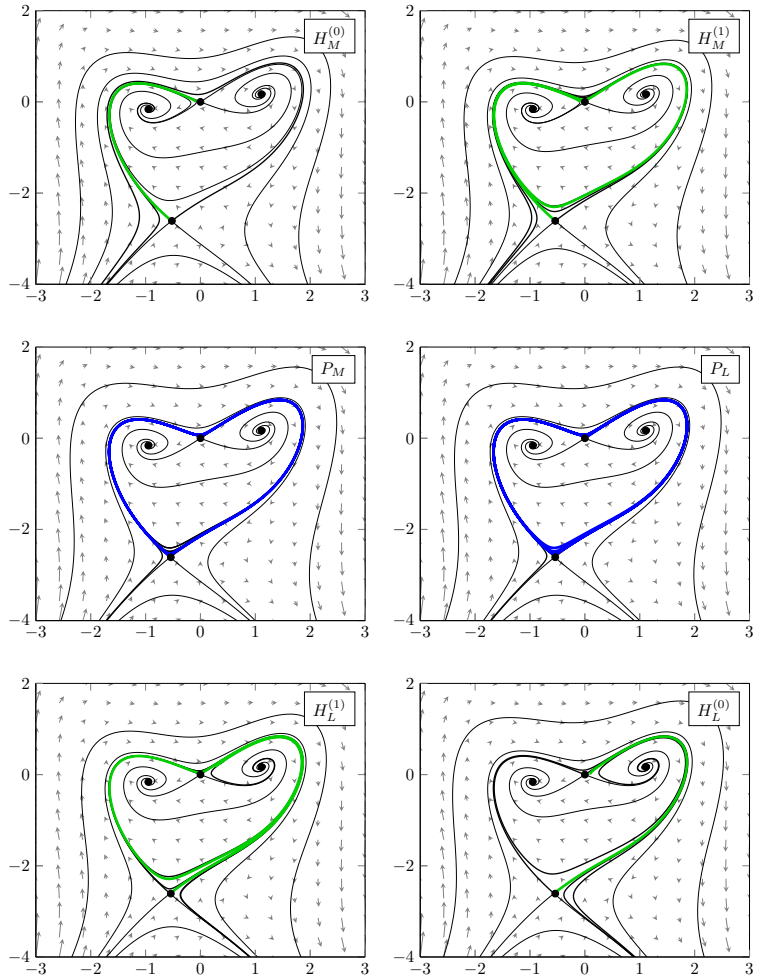

Figure 8.7: Phase portraits for critical values of the parameters

Part V
Discussion

Finally, we discuss some points of improvement and further questions.

The theoretical results collected in this thesis are all derived from the study of truncated model maps. However, it needs further justification that the results obtained from these truncated maps correspond with the results one obtains from the full model maps. More concretely, it must be shown that adding higher order terms to the truncated model maps does not change the results so that the asymptotics of the leading terms are indeed sufficient to obtain all theoretical results. Both theoretical papers [11, 7], on which this thesis is based, deal to some extent with this issue, however a unified treatment is still absent.

In order to complete our collection of examples demonstrating the theoretical results of this thesis, one more example needs to be added. Of the non-monodromic contours, we were only able to produce an example of the simpler subcase (with $\lambda < 1$ and $\mu < 1$). Addition of a non-monodromic example of the other subcase (with $\lambda < 1$ but $\mu > 1$), displaying a fold of cycles bifurcation will complete the stock of examples.

The bifurcations discussed in this thesis all have a semi-local nature. That is, they appear in a neighborhood of a heteroclinic contour. It is often the case that bifurcations which have a global or semi-local nature in systems with few parameters appear locally in systems with more parameters. For example, in [2, 8] the monodromic case is shown to appear close to one case of a degenerate Bogdanov-Takens bifurcation of codim 3. For the non-monodromic case, an analogous result remains to be found. We expect that it must have codimension bigger than 3 and that the linear part of the associated critical normal form is identically zero.

A Parameter tables

For purposes of reproduction, we present a listing of all parameter values used in numerical computation throughout this thesis.

	α	ε
1	0.01	0.01
2	-0.025	0.1
3	-0.1	0.05
4	-0.01	-0.01
5	0.005	-0.01
6	0.01	-0.01

Table 1: Parameter values for Figure 7.6

	α	ε
1	0.02	0.01
2	-0.003	0.3
3	-0.005	0.1
4	-0.005	-0.1
5	0.0025	-1
6	0.006	-1
7	0.001	-0.2

Table 2: Parameter values for Figure 7.7

	α	ε
$H_M^{(0)}$	-0.43	0.38
$H_M^{(1)}$	-0.43	0.3925
P_M	-0.43	0.4025
P_L	-0.43	0.405
$H_L^{(0)}$	-0.43	0.415
$H_L^{(1)}$	-0.43	0.406

Table 3: Parameter values for Figure 8.7

References

[1] V. I. Arnold, V. S. Afrajmovich, Yu. S. Il'yashenko, and L. P. Shil'nikov. *Dynamical Systems V. Bifurcation theory and catastrophe theory*, volume 5 of *Encyclopaedia of Mathematical Sciences*. Springer-Verlag, Berlin, 1994. [A translation of *Current Problems in Mathematics. Fundamental Directions.* Vol. 5, USSR Academy of Sciences, VINITI, Moscow, 1986, in Russian].

[2] A. D. Bazykin, Yu. A. Kuznetsov, and A. I. Khibnik. *Portraits of Bifurcations: Bifurcation diagrams of dynamical systems on the plane*, volume 89 of *Current Life, Science and Technology: Series "Mathematics and Cybernetics"*. "Znanie", Moscow, 1989. [in Russian].

[3] Virginie De Witte, Willy Govaerts, Yuri A. Kuznetsov, and Mark Friedman. Interactive initialization and continuation of homoclinic and heteroclinic orbits in MATLAB. *ACM Trans. Math. Softw.*, 38(3):34, 2012.

[4] B. Deng. The Šil'nikov problem, exponential expansion, strong λ-lemma, C^1-linearization, and homoclinic bifurcation. *J. Differential Equations*, 79(2):189–231, 1989.

[5] A. Dhooge, W. Govaerts, and Yu. A. Kuznetsov. MATCONT: A MATLAB package for numerical bifurcation analysis of ODEs. *ACM Trans. Math. Softw.*, 29(2):141–164, 2003.

[6] A. Dhooge, W. Govaerts, Yu. A. Kuznetsov, H. G.E. Meijer, and B. Sautois. New features of the software matcont for bifurcation analysis of dynamical systems. *Mathematical and Computer Modelling of Dynamical Systems*, 14(2):147–175, 2008.

[7] A. Dukov. Bifurcations of the 'heart' polycycle in generic 2-parameter families. *Transactions of the Moscow Mathematical Society*, 79:1, 11 2018.

[8] F. Dumortier, R. Roussarie, J. Sotomayor, and H. Żołądek. Bifurcations of planar vector fields. Nilpotent singularities and Abelian integrals. *Lect. Notes Math.*, 1480:viii + 226, 1991.

[9] Yu. A. Kuznetsov. *Elements of Applied Bifurcation Theory.* Springer-Verlag, New York, 3rd edition, 2004.

[10] I. P. Malta and J. Palis. Families of vector fields with finite modulus of stability. In D. Rand and L.-S. Young, editors, *Dynamical Systems and Turbulence, Warwick 1980*, pages 212–229, Berlin, Heidelberg, 1981. Springer Berlin Heidelberg.

[11] J. W. Reyn. Generation of limit cycles from separatrix polygons in the phase plane. In R. Martini, editor, *Geometrical Approaches to Differential Equations*, pages 264–289, Berlin, Heidelberg, 1980. Springer Berlin Heidelberg.

[12] B. Sandstede. Constructing dynamical systems having homoclinic bifurcation points of codimension two. *Journal of Dynamics and Differential Equations*, 9:269–288, 04 1997.

[13] L. P. Shilnikov, A. L. Shilnikov, D. Turaev, and L. O. Chua. *Methods of Qualitative Theory in Nonlinear Dynamics. Part II*, volume 5 of *World Scientific Series on Nonlinear Science. Series A: Monographs and Treatises*. World Scientific Publishing Co., Inc., River Edge, NJ, 2001.

[14] S. Sternberg. On the structure of local homeomorphisms of euclidean n-space. II. *Amer. J. Math.*, 80:623–631, 1958.